

A new antibiotic selectively kills Gram-negative pathogens

<https://doi.org/10.1038/s41586-019-1791-1>

Received: 3 April 2019

Accepted: 8 November 2019

Published online: 20 November 2019

There are amendments to this paper

Yu Imai^{1,15}, Kirsten J. Meyer^{1,15}, Akira Iinishi¹, Quentin Favre-Godal¹, Robert Green¹, Sylvie Manuse¹, Mariaelena Caboni¹, Miho Mori¹, Samantha Niles¹, Meghan Ghiglieri¹, Chandrashekhar Honrao², Xiaoyu Ma², Jason J. Guo^{3,3}, Alexandros Makriyannis², Luis Linares-Otoya⁴, Nils Böhringer⁴, Zerlina G. Wuisan⁴, Hundeep Kaur⁵, Runrun Wu^{6,7}, André Mateus⁸, Athanasios Typas⁸, Mikhail M. Savitski⁹, Josh L. Espinoza^{9,10}, Aubrie O'Rourke^{9,10}, Karen E. Nelson^{9,10,11,12}, Sebastian Hiller⁵, Nicholas Noinaj^{6,7}, Till F. Schäberle^{4,13,14}, Anthony D'Onofrio¹ & Kim Lewis^{1*}

The current need for novel antibiotics is especially acute for drug-resistant Gram-negative pathogens^{1,2}. These microorganisms have a highly restrictive permeability barrier, which limits the penetration of most compounds^{3,4}. As a result, the last class of antibiotics that acted against Gram-negative bacteria was developed in the 1960s². We reason that useful compounds can be found in bacteria that share similar requirements for antibiotics with humans, and focus on *Photobacteroides* symbionts of entomopathogenic nematode microbiomes. Here we report a new antibiotic that we name darobactin, which was obtained using a screen of *Photobacteroides* isolates. Darobactin is coded by a silent operon with little production under laboratory conditions, and is ribosomally synthesized. Darobactin has an unusual structure with two fused rings that form post-translationally. The compound is active against important Gram-negative pathogens both in vitro and in animal models of infection. Mutants that are resistant to darobactin map to BamA, an essential chaperone and translocator that folds outer membrane proteins. Our study suggests that bacterial symbionts of animals contain antibiotics that are particularly suitable for development into therapeutics.

It is difficult to find compounds that target Gram-negative bacteria^{1,2}. This problem is largely responsible for the current antimicrobial resistance crisis. Pathogens such as *Escherichia coli*, *Klebsiella pneumoniae*, *Pseudomonas aeruginosa* and *Acinetobacter baumannii* have acquired resistance to most—and in some cases to all—antibiotics that are currently available in the clinic. The WHO (World Health Organization) has recently classified these drug-resistant pathogens as a critical priority for global human health⁵.

Gram-negative bacteria evolved an outer membrane to protect themselves from unwanted compounds^{3,4}. Only a small number of antibiotics can penetrate this barrier, and are active against Gram-negative bacteria.

Most of these compounds are natural products that are made by soil microorganisms, and mainly by Actinomycetes—aminoglycosides, tetracyclines and β-lactams. The last class of antibiotics to act against Gram-negative bacteria, the synthetic fluoroquinolones, were introduced half a century ago. Since then, discovery of

new antibiotics has largely been limited to narrow-spectrum compounds^{2,6}.

We reasoned that useful compounds will be present in microorganisms that have the same requirements for antibiotics as humans. The nematode symbionts *Photobacteroides* and *Xenorhabdus* seem to represent such a group of microorganisms. These nematophilic bacteria are members of the gut microbiome of nematodes and are closely related to other Enterobacteriaceae, such as *E. coli*. Nematodes invade insect larvae and release their symbionts. Nematophilic bacteria first produce neurotoxins to immobilize the prey, and then release various antimicrobials to fend off invading environmental microorganisms^{7,8}. However, the most-direct competitors probably do not come from the environment, but from other members of the nematode gut microbiome. Notably, Gram-negative bacteria that are common opportunistic pathogens of humans are abundant in the microbiome of entomopathogenic nematodes⁹. The antimicrobial compounds produced by nematophilic bacteria must be non-toxic to the nematode, and be able to

¹Antimicrobial Discovery Center, Department of Biology, Northeastern University, Boston, MA, USA. ²Center for Drug Discovery, Department of Pharmaceutical Sciences, Northeastern University, Boston, MA, USA. ³Barnett Institute for Chemical and Biological Analysis, Department of Chemistry and Chemical Biology, Northeastern University, Boston, MA, USA. ⁴Institute for Insect Biotechnology, Justus-Liebig-University of Giessen, Giessen, Germany. ⁵Biozentrum, University of Basel, Basel, Switzerland. ⁶Purdue Institute of Inflammation, Immunology and Infectious Disease, Purdue University, West Lafayette, IN, USA. ⁷Markey Center for Structural Biology, Department of Biological Sciences, Purdue University, West Lafayette, IN, USA. ⁸Genome Biology Unit, European Molecular Biology Laboratory, Heidelberg, Germany. ⁹Department of Human Biology, J. Craig Venter Institute, La Jolla, CA, USA. ¹⁰Department of Genomic Medicine, J. Craig Venter Institute, La Jolla, CA, USA. ¹¹Department of Human Biology, J. Craig Venter Institute, Rockville, MD, USA. ¹²Department of Genomic Medicine, J. Craig Venter Institute, Rockville, MD, USA. ¹³Department of Bioresources, Fraunhofer Institute for Molecular Biology and Applied Ecology, Giessen, Germany. ¹⁴German Center for Infection Research (DZIF), Partner Site Giessen-Marburg-Langen, Giessen, Germany. ¹⁵These authors contributed equally: Yu Imai, Kirsten J. Meyer. *e-mail: k.lewis@neu.edu

Article

spread well through the insect larvae. This suggests the production of antimicrobials with low toxicity and good pharmacokinetics that are active against Gram-negative pathogens.

Identification of darobactin

We screened a small set of *Photobacteroides* and *Xenorhabdus* strains, including a total of 67 isolates from 28 species (Extended Data Table 1), against *E. coli*. Usually, antibiotic-producing bacteria are spotted onto a nutrient agar plate overlaid with a target microorganism. Most of the tested bacteria did not produce zones of inhibition, and we reasoned that this may be due to poor expression of ‘silent’ biosynthetic gene clusters (BGCs) in vitro. We therefore prepared concentrated extracts from the bacterial cultures and spotted them on overlay plates. A concentrated extract from *Photobacteroides khanii* HGB1456 produced a small zone of *E. coli* growth inhibition on a Petri dish, whereas spotting a colony of *P. khanii* HGB1456 had no effect on the growth of *E. coli* (Fig. 1a). Bioassay-guided isolation of the extract by high-performance liquid chromatography produced an active fraction (Extended Data Fig. 1a). High-resolution electrospray ionization–mass spectrometry analysis identified a compound with a molecular mass of 966.41047, which is consistent with a molecular formula of $C_{47}H_{56}O_{12}N_{11}^+$ (calculated $[M + H]^+ = 966.41044$). This mass did not have a match in Antibase, suggesting the presence of a novel compound. Mass-spectrometry fragmentation and nuclear magnetic resonance (NMR) studies (Extended Data Fig. 1b–h) led to the identification of the structure of the active compound, which we named darobactin (Fig. 1b). Darobactin is a modified heptapeptide with an amino acid sequence of $W^1\text{-}N^2\text{-}W^3\text{-}S^4\text{-}K^5\text{-}S^6\text{-}F^7$. NMR studies revealed two unusual macrocycle crosslinks in darobactin: a previously undescribed aromatic–aliphatic ether link between the C7 indole of W^1 and the β -carbon of W^3 , and a carbon–carbon bond between the C6 indole of W^3 and the β -carbon of K^5 . The Trp–Lys bond is made between two unactivated carbons, which has not been described previously for an antibiotic. We next sequenced the genome of *P. khanii* HGB1456 (GenBank accession number WHZZ00000000) and searched for BGCs that encode non-ribosomal peptide synthetases. There were 10 non-ribosomal peptide synthetases in the genome, but none of them could be predicted to form the darobactin peptide. Next, we directly compared the sequence of this seven amino acid peptide with the genome of *P. khanii* and found a perfect match near the C terminus of an open-reading frame that encodes a peptide with a length of 58 amino acids. The ribosomal synthesis of darobactin suggests that the amino acid backbone is in the L-configuration. The macrocycle crosslinks generate two chiral centres at the β -carbons of W^3 and K^5 , which have R and S configurations, respectively, based on nuclear Overhauser effect correlations and molecular modelling (Extended Data Fig. 2).

The putative operon that encodes darobactin (Fig. 1c and Extended Data Fig. 3) is typical of ribosomally synthesized and post-translationally modified peptide genes (RiPPs) that encode a variety of ribosomally produced natural products, including nisin—a food preservative—and the antibiotic thiostrepton. This *dar* operon consists of a propeptide encoded by *darA*, a small *relE*-type open-reading frame, *darBCD*—which encodes an ABC-type trans-envelope exporter (*darB* and *darD* make up the transporter itself, and *darC* encodes a membrane fusion protein)—and *darE*, which encodes a radical S-adenosyl methionine (SAM) enzyme. Enzymes of the radical SAM class catalyse free-radical-based reactions that can link unactivated carbons¹⁰. This explains the formation of the Trp–Lys C–C bond in darobactin. Such a Trp–Lys C–C bond was recently reported in a peptide pheromone, streptide, from *Streptococcus thermophilus*¹¹. There is little overall homology between the two enzymes, but DarE contains the SAM and SPASM domains that are characteristic of this group. The operon does not contain a separate enzyme for generating the ether bond in the first ring. RiPP operons often encode a protease that cleaves out the active peptide; however, this was not present in the *dar* operon. Hence,

Table 1 | MIC and cytotoxicity of darobactin against pathogens, intestinal gut bacteria and human cell lines

Organism and genotype	Concentration ($\mu\text{g ml}^{-1}$)	
	Darobactin	Ampicillin
Pathogenic bacteria (MIC)		
<i>Pseudomonas aeruginosa</i> PAO1	2	>128
<i>Pseudomonas aeruginosa</i> pmrB 523C>T	2	>128
<i>Pseudomonas aeruginosa</i> JMI 1045324	16	ND
<i>Shigella sonnei</i> ATCC 25931 ^a	2	4
<i>Klebsiella pneumoniae</i> ATCC 700603	2	128
<i>Klebsiella pneumoniae</i> ESBL JMI 1052654	2	>128
<i>Klebsiella pneumoniae</i> ATCC 700603 (SHV-18)	4	>128
<i>Klebsiella pneumoniae</i> ATCC BAA-1705 (KPC)	4	>128
<i>Escherichia coli</i> ATCC 25922	2	8
<i>Escherichia coli</i> AR350 (<i>mcr-1</i>)	2	>128
<i>Escherichia coli</i> ESBL JMI 1043856	2	>128
<i>Escherichia coli</i> ATCC BAA-2340 (KPC)	2	>128
<i>Escherichia coli</i> MG1655 +10% serum	2	4
<i>Escherichia coli</i> MG1655	4	4
<i>Salmonella Typhimurium</i> LT2 ATCC 19585 ^a	4	2
<i>Moraxella catarrhalis</i> ATCC 25238 ^a	8	<0.25
<i>Acinetobacter baumannii</i> ATCC 17978	8	64
<i>Enterobacter cloacae</i> ATCC 13047 ^a	32	>128
<i>Proteus mirabilis</i> KLE 2600 ^{a,b}	64	>128
<i>Staphylococcus aureus</i> HG003	>128	0.5
<i>Clostridium bifermentans</i> KLE 2329 ^{a,b}	>128	1
<i>Mycobacterium tuberculosis</i> mc ² 6020	>128	16
Symbiotic gut bacteria (MIC)		
<i>Bifidobacterium longum</i> ATCC BAA-999 ^a	>128	0.25
<i>Bacteroides fragilis</i> ATCC 25285 ^a	>128	128
<i>Bacteroides xylophilus</i> KLE 2253 ^{a,b}	>128	1
<i>Bacteroides dorei</i> KLE 2422 ^{a,b}	>128	1
<i>Bacteroides caccae</i> KLE 2423 ^{a,b}	>128	2
<i>Bacteroides vulgatus</i> KLE 2303 ^{a,b}	>128	2
<i>Bacteroides nordii</i> KLE 2369 ^{a,b}	>128	4
<i>Lactobacillus reuteri</i> ATCC 23272 ^a	>128	1
<i>Enterococcus faecalis</i> KLE 2341 ^{a,b}	>128	4
<i>Faecalibacterium prausnitzii</i> KLE 2243 ^{a,b}	>128	64
<i>Haemophilus parainfluenzae</i> KLE 2367 ^{a,b}	>128	128
<i>Stenotrophomonas maltophilia</i> KLE 11416 ^{a,b}	>128	>128
Human cell line (IC₅₀)		
HepG2	>128	>128
FaDu	>128	>128
HEK293	>128	>128

ND, no data. ESBL, extended spectrum β -lactamase.

^aCultivated under anaerobic conditions.

^bHuman stool isolate, K.L. laboratory collection.

generic proteolysis may be involved in the maturation of the propeptide. To link the putative BGC with production of darobactin, we generated a markerless knockout mutant in which the complete *darABCDE* operon was deleted from *P. khanii* DSM3369 by double crossover. Darobactin production was abolished in the resulting mutant strain (Extended Data Fig. 4a, c, d). Notably, darobactin was produced heterologously from the *dar* operon cloned into *E. coli* (Extended Data Fig. 4b, d). This shows that the *dar* operon is sufficient for making darobactin. Furthermore, it appears that the DarE radical SAM enzyme

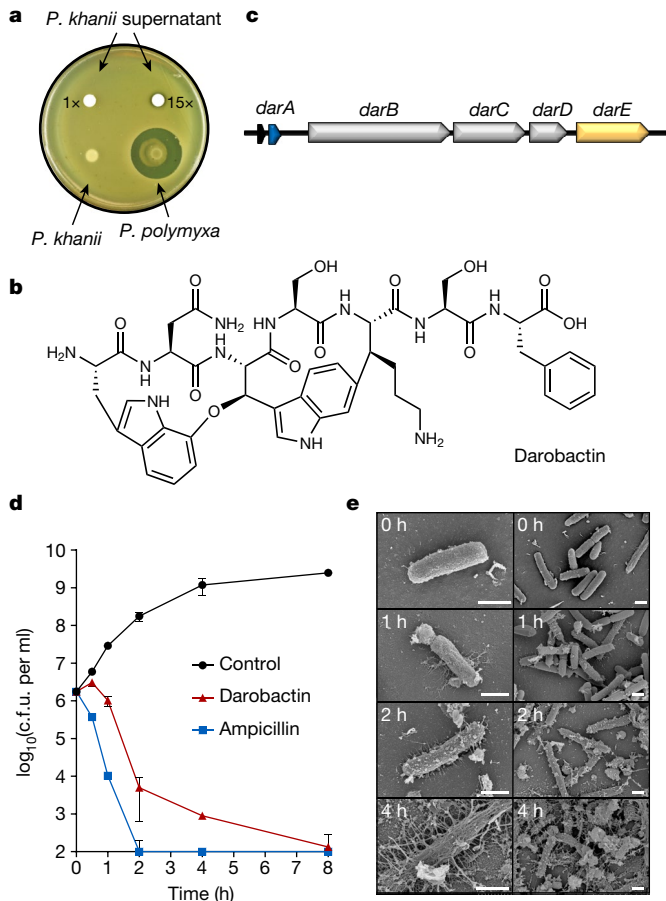


Fig. 1 | Darobactin produced by a silent operon of *P. khanii* is a bactericidal antibiotic. **a**, *P. khanii* was grown in liquid culture, after which concentrated culture supernatants were tested for inhibition of *E. coli* MG1655. The concentrated supernatant of *P. khanii* produced a zone of inhibition on an *E. coli* lawn, whereas unconcentrated supernatant or a colony overlay did not. *Paenibacillus polymyxa* produces polymyxin and serves as a positive control. **b**, Darobactin structure. **c**, The BGC consists of the structural gene *darA* (coloured in blue), *darBCD* (transporter encoding genes; grey) and *darE* (encoding a radical SAM enzyme; orange). In addition, a *relE*-like gene (black) open-reading frame is co-located with the BGC at different positions in different species. **d**, Time-dependent killing of *E. coli* MG1655 by darobactin. An exponential culture of *E. coli* MG1655 was challenged with 16× MIC antibiotics. $n = 3$ biologically independent samples. Data are mean \pm s.d. c.f.u., colony-forming units. **e**, Scanning electron microscopy analysis of *E. coli* MG1655 treated with 16× MIC darobactin. Scale bars, 1 μ m.

catalyses the formation of both the Trp–Lys C–C bond and the C–O–C Trp–Trp ether bond. The chemistries of these two reactions are substantially different, and the mechanism of DarE catalysis requires a separate investigation.

We find that the *dar* operon is common in *Photorhabdus*, and detected it in 15 different species for which the genome sequence is available (Extended Data Fig. 4e). The *dar* operon was absent only in *Photorhabdus bodei*. Synteny of the genomes that contain the *dar* locus with that of *P. bodei* helped to determine the boundaries of the operon (Extended Data Fig. 3a, c). We also tested the production of darobactin in several different *Photorhabdus* species, and found that it is the highest in a strain of *P. khanii* DSM 3369. We switched to this strain for the isolation of darobactin; however, even in this isolate, the production of darobactin is low (3 mg l^{-1}), only twofold higher than in *P. khanii* HGB1456, and requires unusually long fermentation (10–14 days). This probably explains why darobactin has been overlooked in screens for antibiotics.

We then expanded the search for *dar*-type operons in databases of bacterial genome sequences (NCBI), using the propeptide and the *dar*-encoding peptide as queries. The two searches identified homologues of the *dar* operon that appear to encode four darobactin analogues. We therefore propose the name darobactin A for the first compound, and darobactin B–E for the predicted analogues of this class of antibiotics. In *Photorhabdus australis* and *Photorhabdus asymbiotica*, the sequence data suggest the presence of darobactin B, which contains two amino acid changes in the N terminus (SKSF to TKRF). In multiple *Yersinia* species, the second amino acid (N to S), the fifth amino acid (K to R), or both, are modified. We named these analogues darobactin C, D and E, respectively (Extended Data Fig. 4e, f). Notably, the sequence of darobactin C is present in *Yersinia pestis*, the causative agent of the plague, and in *Yersinia frederiksenii* from the human gut microbiome. Darobactin A is the most common, and a corresponding propeptide sequence is present in six sequenced *Photorhabdus* species, seven *Yersinia* species, *Vibrio crassostreeae* and *Pseudoalteromonas luteoviolacea*, all of which are γ -proteobacteria. All species that contain *dar* operons are associated with animals. Apparently, combinatorial reshuffling of the *dar* operon produced a family of genes, and the five analogues were selected over the course of evolution from a total of 1.28×10^9 (20^7) sequences. The GC content of the *dar* operon is 32%, significantly lower than the rest of the genomes of *P. khanii* and other γ -proteobacteria, which have a GC content of 45%. This suggests that the operon was horizontally acquired from a microorganism in which darobactin evolved. Although the nature of this microorganism is unknown, it is not an actinomycete—their genomes have a characteristically high GC content (>55%)¹².

Identifying the target

Darobactin had reasonable activity against a range of Gram-negative bacteria, with a minimum inhibitory concentration (MIC) of $2 \mu\text{g ml}^{-1}$ against important drug-resistant pathogens, *E. coli* and *K. pneumoniae*, including polymyxin-resistant, extended spectrum β -lactamase and carbapenem-resistant clinical isolates (Table 1 and Supplementary Table 1). The compound is bactericidal (Fig. 1d), with a minimal bactericidal concentration of $8 \mu\text{g ml}^{-1}$ against *E. coli*. There was little activity against Gram-positive bacteria. Notably, the compound was also largely inactive against gut commensals, including *Bacteroides*, the main group of Gram-negative symbionts¹³. Disrupting the microbiome by antibiotics, especially early in life, is a major concern, given the important role of symbiotic bacteria in many aspects of human health, such as shaping the immune system during development¹⁴.

Darobactin is a large, 965 Da, molecule, whereas the cut-off for compounds to permeate the outer membrane¹⁵ is around 600 Da. We therefore considered that darobactin, similarly to polymyxin, might target the lipopolysaccharides of the outer membrane. Adding purified lipopolysaccharides to a culture of *E. coli* protected cells from polymyxin, but had no effect on darobactin activity (Extended Data Fig. 5a). Addition of darobactin to *E. coli* caused blebbing of the membrane, and eventual swelling and lysis of cells (Fig. 1e, Extended Data Fig. 6 and Supplementary Video 1). Transcriptome analysis revealed that darobactin rapidly (in 15–30 min) induced the sigma E and Rcs envelope stress responses, and more broadly activated genes from all five envelope stress pathways (Extended Data Fig. 7 and Supplementary Discussion). To identify the target of darobactin, we performed a ligand-protection thermal proteome analysis. This, however, did not reveal a particular protein the denaturation of which was protected by darobactin. At the same time, the proteome showed that the abundance of periplasmic chaperones Spy and DegP was markedly increased, and that the abundance of outer membrane proteins, especially NanC, LamB and OmpF, was decreased (at least in part due to a decrease in the respective transcripts) in response to darobactin treatment (Extended Data Fig. 8, Supplementary Table 2 and Supplementary Discussion). Microscopy, transcriptome and proteome

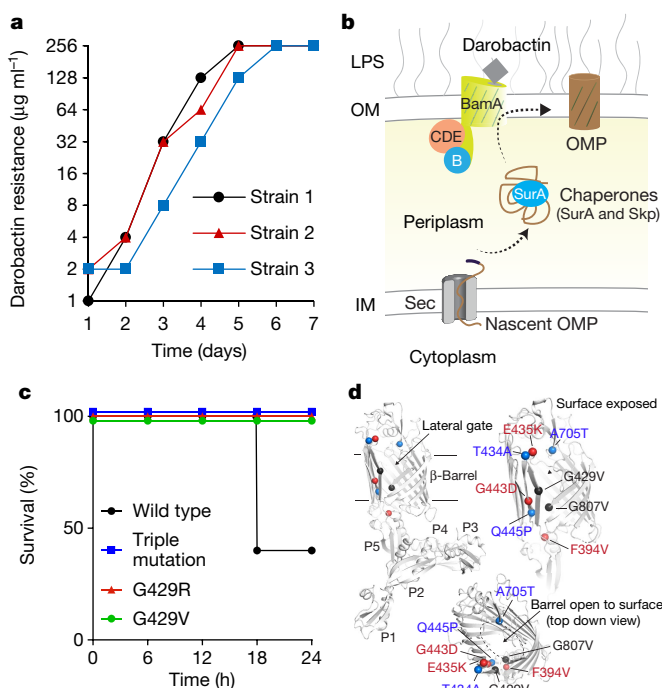


Fig. 2 | Multiple mutations in *bamA* confer darobactin resistance.

a, Darobactin-resistant mutants were generated by daily serial passage of *E. coli* MG1655 at sub-MIC concentrations of darobactin, leading to a steady shift in the darobactin concentration that permits *E. coli* MG1655 growth. This experiment was performed in three biologically independent samples. The three mutants obtained contained 2–3 mutations in *bamA*. **b**, Schematic of the Bam complex³⁷. IM, inner membrane; OM, outer membrane. **c**, Mice were injected with 10^7 c.f.u. of *E. coli* ATCC 25922 wild-type or darobactin-resistant strains. Resistant strains carried either; the triple mutations evolved in strain 3 (**a**), or single spontaneous mutations of G429 to R or V. *n* = 5 per group. Mice were monitored for survival. **d**, Darobactin-resistance mutations (coloured spheres) mapped to the BamA protein structure (grey) shown as a cartoon with the β-barrel domain and the individual polypeptide-transport-associated domains indicated.

analyses indicate a defect in the cell envelope. We next sought to obtain mutants that were resistant to darobactin to identify its target. Plating *E. coli* on solid medium that contained darobactin at 4× MIC produced resistant mutants with a frequency of 8×10^{-9} . To obtain mutants that were resistant to higher levels of the compound, we performed an evolutionary experiment in liquid medium¹⁶ (Fig. 2a). Repeatedly re-inoculating a culture into medium with progressively increasing levels of the antibiotic produced mutants with a high resistance to darobactin, which had MICs greater than $128 \mu\text{g ml}^{-1}$ (Fig. 2a). Sequencing the mutants showed that in all three strains of *E. coli*, there were 2–3 mutations in the gene that encodes BamA, an essential outer membrane protein¹⁷ (Fig. 2b). After transferring the three *bamA* mutations from the resistant strain 3 to a clean *E. coli* background by allelic replacement, we confirmed that they are solely responsible for darobactin resistance (MIC of $128 \mu\text{g ml}^{-1}$). The ability to generate mutants that are resistant to high levels of the compound suggests a lack of off-target activity. To sustain an infection in the presence of an antibiotic, the pathogen should be both resistant and virulent. We therefore tested whether darobactin-resistant mutants retained virulence. Injecting mice with 10^7 cells of *E. coli* ATCC 25922 caused 60% mortality within 24 h. By contrast, there was no death at 24 h when the animals were inoculated with *E. coli* carrying either single or triple mutations in *bamA* (Fig. 2c and Extended Data Fig. 5b). *E. coli* virulence is thus strongly compromised by *bamA* mutations that confer resistance to darobactin.

BamA is the central component of the BamABCDE complex¹⁷ (Fig. 2b). One proposed mechanism for BAM is that nascent outer membrane proteins are inserted from the periplasm into the outer membrane by the central component BamA, which serves to catalyse both folding and insertion. BamA is not an enzyme, and its β-barrel structure does not obviously lend itself to inhibition by small molecules. BamA is targeted by large lectin-like bacteriocins, LlpA¹⁸, and a group from Genentech developed an antibody that inhibits this protein in *E. coli*¹⁹. In a recent study, a small molecule synthetic compound MRL-494 was reported to act against BamA, without the need to penetrate the outer membrane²⁰. MRL-494 is active against *E. coli* and *K. pneumoniae* with an MIC of 15 and $62 \mu\text{g ml}^{-1}$, respectively, whereas it acts against Gram-positive bacteria by disrupting their cytoplasmic membrane.

We observed direct inhibition of BAM by darobactin using an in vitro protein refolding assay. The isolated BAM complex was integrated into lipid nanodiscs, and its ability to fold the protease OmpT was measured (Extended Data Fig. 5c). Darobactin inhibited BAM-dependent folding of OmpT with an apparent half-maximum inhibitory concentration (IC_{50}) of $0.68\text{--}1 \mu\text{M}$ (Fig. 3a and Extended Data Fig. 5d), consistent with the MIC of $1.9 \mu\text{M}$ in *E. coli*. Darobactin had no effect on OmpT activity in the absence of BAM (Extended Data Fig. 5e), and a linear peptide with the same sequence as darobactin had no inhibitory activity on BAM (Extended Data Fig. 5f). We next tested darobactin-resistant mutants in the same assay. The IC_{50} of mutant 1a was increased markedly, to $120 \mu\text{M}$. In mutants 2 and 3, the IC_{50} was unchanged, but the folding activity was strongly decreased (Fig. 3a). The mechanism by which mutants 2 and 3 confer resistance is unclear and will require additional study.

Using isothermal titration calorimetry experiments, we also observed that darobactin directly and specifically interacts with BamA of BAM with a measured dissociation constant (K_d) of $1.2 \mu\text{M}$, with no binding observed for the linear peptide (Fig. 3b and Extended Data Fig. 5g, h).

To characterize the interaction of BamA with darobactin at the atomic level, we performed a high-resolution NMR study. Stepwise titration of the unlabelled darobactin with the [^{15}N , ^2H]-labelled BamA β-barrel (BamA-β) was carried out and monitored by solution NMR spectroscopy. Upon addition of 0.5-molar-equivalent darobactin, significant changes were observed in the NMR spectrum of BamA-β, which became more prominent at 1 molar equivalent (Extended Data Fig. 5i and Supplementary Data 1). By contrast, a linear scrambled darobactin peptide had no effect on the NMR spectrum (Extended Data Fig. 5j and Supplementary Data 1). We have previously shown that BamA-β exists as an interchanging two-state ensemble of a gate-closed and a gate-opened conformation and that each of these two conformations can be stabilized by a conformation-specific nanobody, nanoF7 for the gate-closed and nanoE6 for the gate-opened structure^{21,22}. Notably, we found that darobactin stabilized one of these two conformations (Fig. 3c, d). The darobactin-stabilized conformation resembles for most residues the closed-gate conformation, as shown by the high similarity of NMR spectral positions of BamA-β and nanoF7 and BamA-β and darobactin, whereas the NMR position of BamA-β and nanoE6 was clearly different (Fig. 3c, d). These findings strongly suggest that darobactin stabilizes a closed lateral gate upon binding to BamA, preventing the exit of substrates into the outer membrane. Notably, most mutations that confer resistance to darobactin are located at the lateral gate of BamA (Fig. 2d). Taken together, these findings are consistent with darobactin inhibiting BamA and disrupting the formation of a functional outer membrane. Future studies will determine the mechanism by which darobactin kills bacterial cells by acting against this target.

Animal efficacy

Given the attractive mode of action and lack of cytotoxicity (Table 1), we next examined the efficacy of darobactin in mouse models of infection. Single-dose pharmacokinetic analysis shows that darobactin achieves good exposure, with an intraperitoneal injection of 50 mg kg^{-1} leading

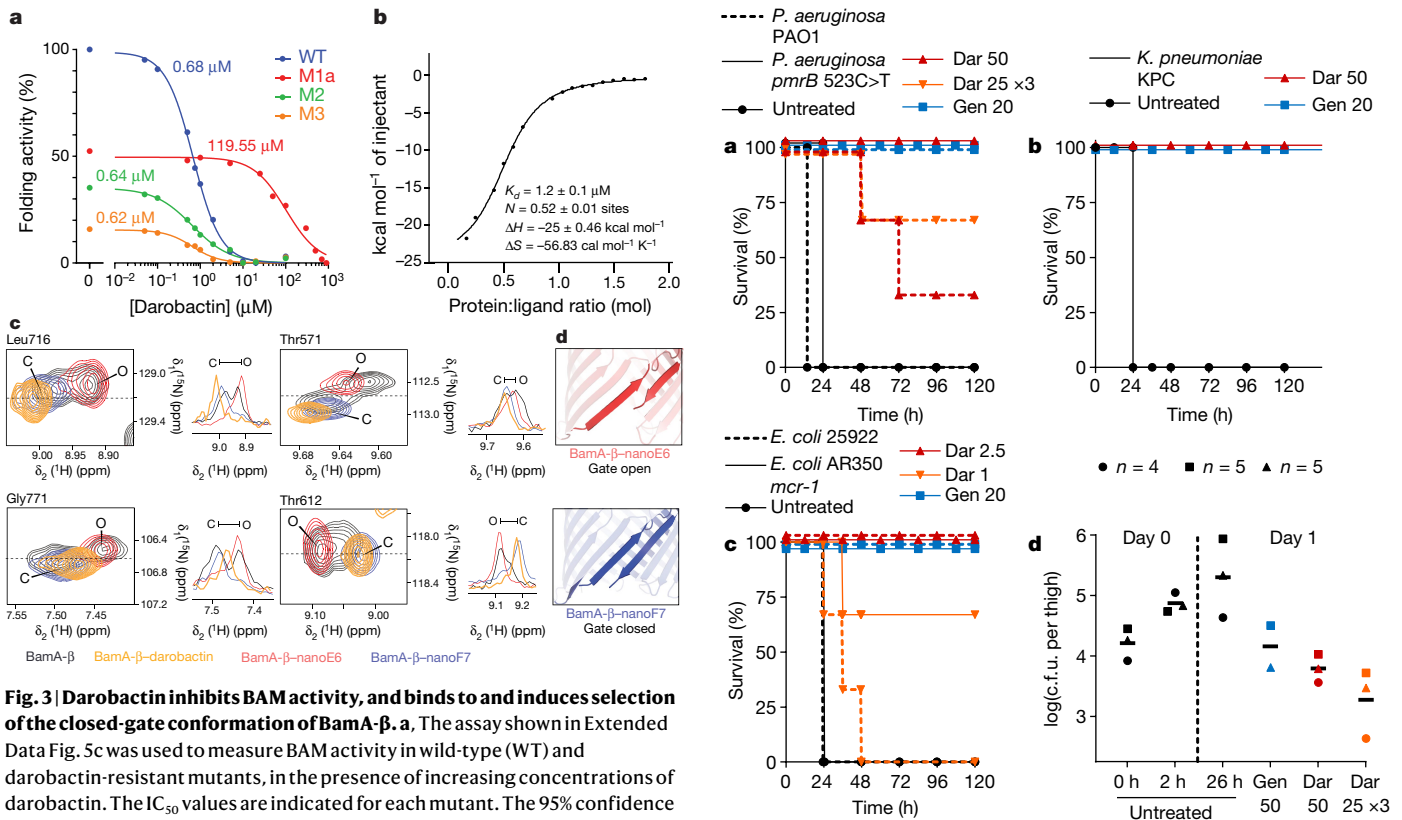
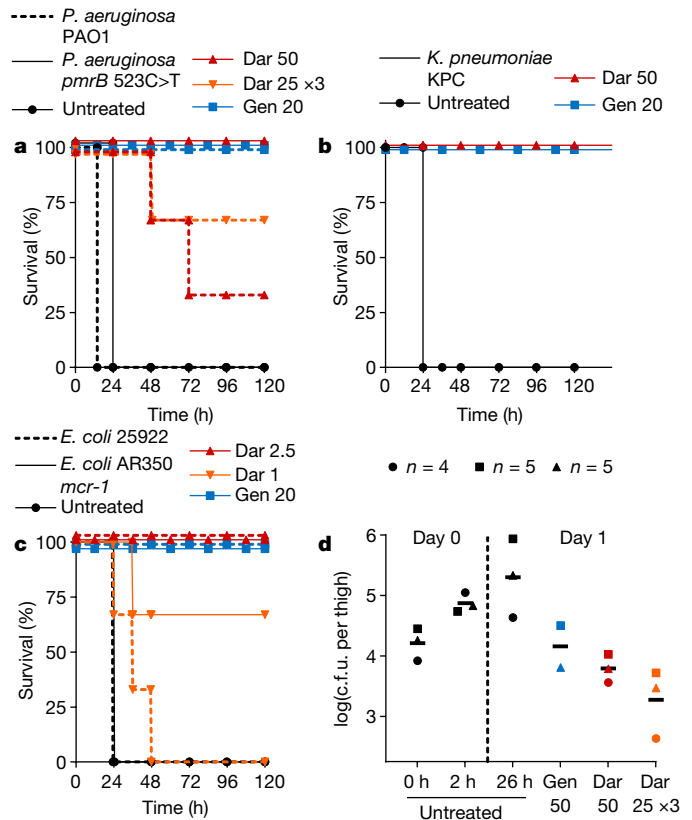


Fig. 3 | Darobactin inhibits BAM activity, and binds to and induces selection of the closed-gate conformation of BamA-β. **a**, The assay shown in Extended Data Fig. 5c was used to measure BAM activity in wild-type (WT) and darobactin-resistant mutants, in the presence of increasing concentrations of darobactin. The IC_{50} values are indicated for each mutant. The 95% confidence intervals for the IC_{50} are: wild type 0.61–0.75 μ M, M1a (G429V, T434A and G807V; Methods) 68–148 μ M, M2 (F394V, E435K and G443D) 0.50–0.83 μ M, M3 (T434A, Q445P and A705T) 0.38–0.94 μ M (GraphPad Prism v.8.2). The experiment was repeated independently at least three times with similar results. **b**, Specific binding of darobactin to BamA/BAM. Plot of isothermal titration calorimetry experiments of wild-type BAM titrated with darobactin. $K_d = 1.2 \pm 0.1 \mu$ M, $N = 0.52 \pm 0.01$ sites, $\Delta H = -25 \pm 0.46 \text{ kcal mol}^{-1}$ and $\Delta S = -56.83 \text{ cal mol}^{-1} \text{ K}^{-1}$. The experiment was repeated independently twice with similar results. **c**, Two-dimensional magnification and one-dimensional cross-sections from two-dimensional [^{15}N , ^1H]-TROSY spectra of BamA-β in lauryldimethylamine-N-oxide micelles for four selected amino acid residues, as indicated at the top of each panel. Apo BamA-β (black), equimolar BamA-β-darobactin (orange), BamA-β-nanoF7 (blue) and BamA-β-nanoE6 (red). Resonances that correspond to the open and closed conformation are indicated as O and C, respectively. The experiment was repeated independently twice with similar results. **d**, Conformation of the gate region in crystal structures of BamA-β-nanoE6 and BamA-β-nanoF7 (Protein Data Bank (PDB) 6QGW and 6QGX7, respectively).

to a peak blood level of 94 μ g ml $^{-1}$ and a half-life of 1 h (Extended Data Fig. 9a). Notably, the blood levels of the compound were maintained above the MIC of *E. coli* for 8 h, an excellent predictor of efficacy. We also did not notice any toxicity with this dose of darobactin. Next, the efficacy of the compound was examined in a mouse septicemia model. For this, we examined wild-type and polymyxin-resistant *P. aeruginosa* (PAO1 and *pmrB* 523C>T), carbapenemase-producing *K. pneumoniae* (KPC), and wild-type and polymyxin-resistant *E. coli* (ATCC 25922 and AR350 *mcr-1*) (Fig. 4a–c). Carbapenem-resistant *K. pneumoniae* causes 30–40% mortality in the United States and 40–50% in Europe^{23,24}. Polymyxin-resistant *E. coli mcr-1* is of particular concern, as the resistance locus is present on a plasmid and can rapidly spread²⁵.

To initiate septicemia, mice were infected intraperitoneally and 1 h after introducing the pathogens, darobactin was administered. Untreated controls all died within 24 h, but a single dose of darobactin completely protected the animals infected with *E. coli*, *K. pneumoniae* and polymyxin-resistant *P. aeruginosa* (Fig. 4a–c). Darobactin given in three doses of 25 mg kg $^{-1}$ cured two out of three mice infected with



wild-type *P. aeruginosa* PAO1 (Fig. 4a). Darobactin was then tested in a mouse thigh infection with *E. coli mcr-1*. In this model, animals were made neutropenic with cyclophosphamide treatment, and the ability of the antibiotic to kill the pathogen is tested in the absence of an immune response. Darobactin, given as either a single injection of 50 mg kg $^{-1}$ or as three injections of 25 mg kg $^{-1}$ every 6 h, significantly decreased the pathogen burden at 26 h, and was more efficacious than gentamicin (50 mg kg $^{-1}$) (Fig. 4d and Extended Data Fig. 9b). These experiments suggest that darobactin is a promising lead compound for developing a therapeutic against Gram-negative pathogens.

Discussion

The number of novel compounds that target Gram-negative bacteria is small, comprising mainly β -lactamase inhibitors—avibactam²⁶, vaborbactam²⁷ and aspergillomarasmine²⁸; arylomycin analogues that target the LepB signal peptidase²⁹ are in development by Genentech³⁰.

An intriguing new discovery platform is in development, based on emerging rules of permeation that determine the properties that are required for compounds to breach the permeability barrier

Article

of Gram-negative bacteria³¹. However, perhaps the most-practical approach is currently to mine untapped groups of microorganisms that may harbour new chemistry. These include uncultured bacteria, from which teixobactin was discovered¹⁶; and several of the most abundant soil taxa—Acidobacteria, Verrucomicrobia, Rokubacteria and Gemmatimonadetes³². Several dozen compounds with antimicrobial properties have been isolated from nematophiles³³, but only the odilorhabdins (produced by *Xenorhabdus nematophila*) hit a specific target and show efficacy in certain animal models of infection^{34,35}. The currently identified compounds represent a small fraction of what is encoded by the genomes of nematophilic bacteria and are expressed well under laboratory conditions; darobactin is encoded by a silent operon. Nematophilic bacteria split from other Enterobacteriaceae around 370 million years ago³⁶. Since then, they would have acquired, by horizontal transmission from the biosphere, antibiotics that may be of use to us.

Darobactin is indeed a typical example of a compound that is acquired by horizontal transmission of a BGC operon from an unknown microorganism. It acts against an attractive target on the surface of the cell. The BamA chaperone, which is itself an outer membrane β-barrel protein, catalyses folding and insertion of new β-barrel proteins into the outer membrane. Drugs in general, and natural products in particular, normally target enzymes with their well-defined catalytic centres, rather than chaperones. According to our data, darobactin stabilizes the closed lateral gate conformation of BamA, preventing it from opening and inserting its substrates into the membrane. Darobactin is a large molecule, which is probably necessary for its unusual mode of action. The location of the target on the surface resolves the intractable problem of penetration across the permeability barrier of Gram-negative bacteria. There are only two essential proteins exposed on the surface of the outer membrane—BamA and LptD¹⁷. There is little doubt that nature produced more than one type of compounds that acts against these targets.

Online content

Any methods, additional references, Nature Research reporting summaries, source data, extended data, supplementary information, acknowledgements, peer review information; details of author contributions and competing interests; and statements of data and code availability are available at <https://doi.org/10.1038/s41586-019-1791-1>.

1. Payne, D. J., Gwynn, M. N., Holmes, D. J. & Pompili, D. L. Drugs for bad bugs: confronting the challenges of antibiotic discovery. *Nat. Rev. Drug Discov.* **6**, 29–40 (2007).
2. Lewis, K. Platforms for antibiotic discovery. *Nat. Rev. Drug Discov.* **12**, 371–387 (2013).
3. Lomovskaya, O. & Lewis, K. emr, an *Escherichia coli* locus for multidrug resistance. *Proc. Natl Acad. Sci. USA* **89**, 8938–8942 (1992).
4. Li, X. Z. & Nikaido, H. Efflux-mediated drug resistance in bacteria. *Drugs* **64**, 159–204 (2004).
5. Tacconelli, E. et al. Discovery, research, and development of new antibiotics: the WHO priority list of antibiotic-resistant bacteria and tuberculosis. *Lancet Infect. Dis.* **18**, 318–327 (2018).
6. Brown, E. D. & Wright, G. D. Antibacterial drug discovery in the resistance era. *Nature* **529**, 336–343 (2016).
7. Crawford, J. M. & Clardy, J. Bacterial symbionts and natural products. *Chem. Commun.* **47**, 7559–7566 (2011).
8. Tobias, N. J., Shi, Y. M. & Bode, H. B. Refining the natural product repertoire in entomopathogenic bacteria. *Trends Microbiol.* **26**, 833–840 (2018).
9. Tambong, J. T. Phylogeny of bacteria isolated from *Rhabditis* sp. (Nematoda) and identification of novel entomopathogenic *Serratia marcescens* strains. *Curr. Microbiol.* **66**, 138–144 (2013).
10. Yokoyama, K. & Lilla, E. A. C-C bond forming radical SAM enzymes involved in the construction of carbon skeletons of cofactors and natural products. *Nat. Prod. Rep.* **35**, 660–694 (2018).
11. Schramma, K. R., Bushin, L. B. & Seyedsayamost, M. R. Structure and biosynthesis of a macrocyclic peptide containing an unprecedented lysine-to-tryptophan crosslink. *Nat. Chem.* **7**, 431–437 (2015).
12. Embley, T. M. & Stackebrandt, E. The molecular phylogeny and systematics of the actinomycetes. *Annu. Rev. Microbiol.* **48**, 257–289 (1994).
13. Lloyd-Price, J., Abu-Ali, G. & Huttenhower, C. The healthy human microbiome. *Genome Med.* **8**, 51 (2016).
14. Bokulich, N. A. et al. Antibiotics, birth mode, and diet shape microbiome maturation during early life. *Sci. Transl. Med.* **8**, 343ra82 (2016).
15. O’Shea, R. & Moser, H. E. Physicochemical properties of antibacterial compounds: implications for drug discovery. *J. Med. Chem.* **51**, 2871–2878 (2008).
16. Ling, L. L. et al. A new antibiotic kills pathogens without detectable resistance. *Nature* **517**, 455–459 (2015).
17. Konovalova, A., Kahne, D. E. & Silhavy, T. J. Outer membrane biogenesis. *Annu. Rev. Microbiol.* **71**, 539–556 (2017).
18. Ghequire, M. G. K., Swings, T., Michiels, J., Buchanan, S. K. & De Mot, R. Hitting with a BAM: selective killing by lectin-like bacteriocins. *mBio* **9**, e02138-17 (2018).
19. Stork, K. M. et al. Monoclonal antibody targeting the β-barrel assembly machine of *Escherichia coli* is bactericidal. *Proc. Natl Acad. Sci. USA* **115**, 3692–3697 (2018).
20. Hart, E. M. et al. A small-molecule inhibitor of BamA impervious to efflux and the outer membrane permeability barrier. *Proc. Natl Acad. Sci. USA* **116**, 21748–21757 (2019).
21. Hartmann, J.-B., Zahn, M., Burmann, I. M., Bibow, S. & Hiller, S. Sequence-specific solution NMR assignments of the β-barrel insertase BamA to monitor its conformational ensemble at the atomic level. *J. Am. Chem. Soc.* **140**, 11252–11260 (2018).
22. Kaur, H. et al. Identification of conformation-selective nanobodies against the membrane protein insertase BamA by an integrated structural biology approach. *J. Biomol. NMR* **73**, 375–384 (2019).
23. Ramos-Castañeda, J. A. et al. Mortality due to KPC carbapenemase-producing *Klebsiella pneumoniae* infections: systematic review and meta-analysis: mortality due to KPC *Klebsiella pneumoniae* infections. *J. Infect.* **76**, 438–448 (2018).
24. Xu, L., Sun, X. & Ma, X. Systematic review and meta-analysis of mortality of patients infected with carbapenem-resistant *Klebsiella pneumoniae*. *Ann. Clin. Microbiol. Antimicrob.* **16**, 18 (2017).
25. Sun, J., Zhang, H., Liu, Y. H. & Feng, Y. Towards understanding MCR-like colistin resistance. *Trends Microbiol.* **26**, 794–808 (2018).
26. Levasseur, P. et al. Efficacy of a ceftazidime–avibactam combination in a murine model of septicemia caused by Enterobacteriaceae species producing ampc or extended-spectrum β-lactamases. *Antimicrob. Agents Chemother.* **58**, 6490–6495 (2014).
27. Wunderink, R. G. et al. Effect and safety of meropenem–vaborbactam versus best-available therapy in patients with carbapenem-resistant Enterobacteriaceae infections: the TANGO II randomized clinical trial. *Infect. Dis. Ther.* **7**, 439–455 (2018).
28. King, A. M. et al. Aspergillomarasmine A overcomes metallo-β-lactamase antibiotic resistance. *Nature* **510**, 503–506 (2014).
29. Liu, J., Smith, P. A., Steed, D. B. & Romesberg, F. Efforts toward broadening the spectrum of arylomycin antibiotic activity. *Bioorg. Med. Chem. Lett.* **23**, 5654–5659 (2013).
30. Smith, P. A. et al. Optimized arylomycins are a new class of Gram-negative antibiotics. *Nature* **561**, 189–194 (2018).
31. Richter, M. F. et al. Predictive compound accumulation rules yield a broad-spectrum antibiotic. *Nature* **545**, 299–304 (2017).
32. Crits-Christoph, A., Diamond, S., Butterfield, C. N., Thomas, B. C. & Banfield, J. F. Novel soil bacteria possess diverse genes for secondary metabolite biosynthesis. *Nature* **558**, 440–444 (2018).
33. Tobias, N. J. et al. Natural product diversity associated with the nematode symbionts *Photorhabdus* and *Xenorhabdus*. *Nat. Microbiol.* **2**, 1676–1685 (2017).
34. Pantel, L. et al. Odilorhabdins, antibacterial agents that cause miscoding by binding at a new ribosomal site. *Mol. Cell* **70**, 83–94.e7 (2018).
35. Racine, E. et al. In vitro and in vivo characterization of NOSO-502, a novel inhibitor of bacterial translation. *Antimicrob. Agents Chemother.* **62**, e01016–e01018 (2018).
36. Poinar, G. Jr. Origins and phylogenetic relationships of the entomophilic rhabditids, *Heterorhabditis* and *Steinernema*. *Fundam. Appl. Nematol.* **16**, 333–338 (1993).
37. Bakalar, J., Buchanan, S. K. & Noinaj, N. The structure of the β-barrel assembly machinery complex. *Science* **351**, 180–186 (2016).

Publisher’s note Springer Nature remains neutral with regard to jurisdictional claims in published maps and institutional affiliations.

© The Author(s), under exclusive licence to Springer Nature Limited 2019

Methods

Screening conditions

Photobacterium and *Xenorhabdus* strains used in this study were purchased from Deutsche Sammlung von Mikroorganismen und Zellkulturen (DSMZ) or provided by H. Goodrich-Blair. Strains were inoculated in 10 ml Luria–Bertani (LB) broth in 50-ml Falcon tubes and incubated overnight, then diluted 1:100 in new Falcon tubes with 10 ml LB broth, nutrient broth or tryptic soy broth and incubated for 8 days, at 28 °C with shaking at 200 rpm. Culture aliquots (1 ml) were centrifuged at 12,000g for 10 min, and supernatants (750 µl) were collected and dried by centrifugal evaporation. Dried samples were resuspended in 50 µl Milli-Q water or 50% dimethyl sulfoxide to generate 15× concentrated extracts, then 3 µl was spotted onto *E. coli* overlays. Overlays were prepared from an exponential culture of *E. coli* (grown for 2–5 h after dilution of 1:100 from an overnight culture in cation-adjusted Mueller Hinton II broth (MHIIIB) and incubated at 37 °C with shaking at 220 rpm), diluted to an optical density at 600 nm (OD_{600}) of 0.03 in MHIIIB. These cultures were used to cover cation-adjusted Mueller Hinton II agar (MHIIA) plates; the excess culture was removed and overlays were left to dry in a biosafety cabinet. Overlays spotted with culture extracts were incubated at 37 °C overnight and the activity was evaluated by zones of inhibition.

Strain fermentation and purification of darobactin

P. khanii strains were inoculated in a 500-ml Erlenmeyer flask with 200 ml LB broth and incubated at 28 °C with aeration at 200 rpm overnight, then diluted 1:100 into a 2-l Erlenmeyer flask with 1 l tryptic soy broth and incubated for 10–14 days. Cells were removed by centrifugation at 8,000g for 10 min, and the culture supernatant was incubated overnight with XAD16N resin (20–60 mesh, Sigma-Aldrich), under agitation, to bind darobactin. Darobactin was eluted from the XAD16N resin using 1 l of 50% methanol with 0.1% formic acid. The eluate was concentrated using a rotary evaporator, and subjected to cation-exchange (SP Sepharose XL, GE Healthcare) chromatography. The concentrated eluate was loaded on to the activated cation-exchange resin and the resin washed with 0.1% (v/v) formic acid in ddH₂O. The compound was eluted by step gradients of 50 mM ammonium acetate pH 5, pH 7 and pH 8. The bioactive eluates were combined and freeze-dried, then resuspended in 0.1% (v/v) formic acid in Milli-Q water. The solution was subjected to reverse-phase high-performance liquid chromatography (RP-HPLC) on a C18 column (Agilent, C18, 5 µm; 250 mm × 10 mm, Restek). HPLC conditions were as follows: solvent A, Milli-Q water and 0.1% (v/v) formic acid; solvent B, acetonitrile and 0.1% (v/v) formic acid. The initial concentration of 2% solvent B was maintained for 2 min, followed by a linear gradient to 26% over 12 min with a flow rate of 5 ml min⁻¹; UV detection by diode-array detector from 210 to 400 nm. Darobactin was eluted at 12.5 min, with a purity of 97% by UV.

Structure elucidation

Mass spectrometric analysis. The exact mass of darobactin was determined using a Q Exactive Hybrid Quadrupole-Orbitrap Mass Spectrometer (Thermo Scientific) equipped with a heated electrospray ionization source operated in positive ionization mode. Darobactin was prepared in Milli-Q water and 0.1% formic acid and introduced into the mass spectrometer by direct infusion at a constant flow rate of 5 µl min⁻¹. The ion source conditions were set as follows: ion spray voltage, 1.50 kV; capillary temperature, 125 °C; spray current, 50 µA; sheath gas, O₂; and aux gas, 2. The tandem mass spectrometry (MS/MS) spectrum for darobactin was acquired in higher-energy collisional dissociation mode and a collision energy of 55 eV was applied for the fragmentation. The mass analyser was calibrated according to the manufacturer's directions. Data acquisition and processing were performed using Xcalibur software (Thermo Fisher Scientific).

NMR studies. All NMR data were recorded on a Bruker AVANCE II 700-MHz NMR spectrometer with 5 mm TXI probehead and a Bruker AVANCE NEO 600-MHz NMR spectrometer equipped with a 5 mm TCI cryoprobe. Complete assignments were obtained using two-dimensional experiments, including COSY (cosydfesgpphp), TOCSY (dipsi2esfbgpph), ¹H-¹⁵N HSQC (hsqcetfpf3gpsi), ¹H-¹³C HSQC (hsqcedetgpsisp2.3), ¹H-¹³C HMBC (hmbcgp1pnprqf) and ROESY (roesyesgpph). All NMR experiments were performed with 5 mg of darobactin solubilized in 500 µl of aqueous solvent containing 94% (v/v) Milli-Q water, 4% (v/v) deuterium oxide and 2% (v/v) deuterated formic acid. Additional ¹D-¹H and ²D HMBC and ROESY NMR experiments were performed with 5 mg of darobactin solubilized in 500 µl of 2:1 (v/v) mixture of Milli-Q water and deuterated acetonitrile, including 2% (v/v) deuterated formic acid.

Modelling of isomers. Modelling of the four possible darobactin isomers was performed in Schrödinger 2018-2. The four isomers first underwent conformational search in the Macromodel module (Schrödinger) with MMFF forcefield. Mixed torsional/low-mode sampling method was used with a maximum of 10,000 steps. The lowest energy conformer for each isomer was then subjected to geometry optimization using Jaguar (Schrödinger) at B3LYP/6-31G (d, p) level with fine-grid density and the ultrafine accuracy level of SCF. All simulations were performed for gas phase.

Identification of the BGC

The genome of *P. khanii* HGB1456 was sequenced by both Pacbio technology and Illumina MiSeq, and assembled using SPAdes 3.11³⁸. The resulting data were initially analysed using antibiotic and secondary metabolite analysis shell (antiSMASH³⁹). Each predicted BGC was then analysed manually, taking into account the number and identity of predicted amino acids. As this initial approach did not yield any putative darobactin BGCs, a direct screening for the core peptide sequence WNWSKF was done on all *Photobacterium* genomes available in public databases using the Basic Local Alignment Search Tool (BLAST). In *P. khanii*, the seven amino acid sequence of darobactin was located close to the C terminus of an open-reading frame that encodes 58 amino acids, upstream of an ABC transporter and a radical SAM enzyme, suggesting a RiPP operon. This putative BGC was identified in the other darobactin producers *P. luminescens* DSM3368 and *P. khanii* DSM3369. The boundaries of the cluster were determined by comparison with the *P. bodei* genome, which did not contain the operon. Furthermore, the GC content of the *dar* cluster was clearly lower than the rest of the average GC content in the genome (32% versus 45%).

To identify other bacterial species that potentially produced darobactin-like compounds, homologous enzymes were searched using the radical SAM protein sequence (DarE) as input in BLAST. The genomic context of each hit was analysed manually to confirm the presence of a DarA-like propeptide in the vicinity of the radical SAM protein. In addition, a search using the propeptide DarA as input was done, delivering the same hits.

Generation of a darobactin deletion mutant and heterologous expression

To delete the *dar* BGC (*darABCDE*) from the genome of the producer strain *P. khanii* DSM3369, a plasmid was constructed by assembly of five fragments, which enables markerless genome modification. Chromosomal DNA was isolated using the innuprepBacteria DNA Kit (AnalytikJena). Fragments up- and downstream of the BGC were amplified (size of around 1 kb) using the primer pairs 5'-TTGACGTTGGACTCCACGTG TTATGGACGTGGCAAACCGGGTCTTGAC-3', 5'-TTGAAATATCAGGATA GCATTGCGCTCGCTCACCCCCGTACATAGTCG-3'; and 5'-ATGCTA TCCTGATATTCAAATGCAAGTAAAATGTTCATCATAATAACC-3' and 5'-TTCTGACGAGTCTCTGAGATGGGTTGATATCCACTGATATAAAC-3'. Then, the R6K origin of replication (ori), the origin of transfer

Article

(oriT) and the levan sucrase gene *sacB* from *Bacillus subtilis* were amplified in one piece from the vector pNPTS138⁴⁰ using the primers 5'-TCGAGCTCAAGGAGGTATAAAAATGAACATCAAAAGTTGCAA AACAGCA-3' and 5'-ACGTGGACTCCAACGTCAA-3'. Next, the arabinose-inducible expression system of pKD46⁴¹ with the adjacent β -lactamase (*bla*) promoter was amplified using the primers 5'-ACTCTCCTTTCAATATTGAAGCAT-3' and 5'-TCGATTTTT ATAACCTCCTTAGAGCTCGAATTCC-3'. Finally, the *aph* gene from pCAP03⁴², which confers resistance to kanamycin, was amplified using the primers 5'-TCAGAAGAACCTCGTAAGAAGGCCA-3' and 5'-TCAATAATTGAAAAAGGAAGAGTATGATTGAACAAGATGGATTGC ACG-3'. All fragments were amplified by Q5 DNA polymerase (New England Biolabs), the gel was purified with 1% or 2% TAE agarose gels and the DNA was retrieved with the Large Fragment DNA Recovery Kit (Zymo Research). Subsequently all fragments were fused by isothermal assembly, generating the plasmid pNB02.

After assembly, *E. coli* WM3064 cells were transformed with pNB02 by electroporation and correct assembly was corroborated by PCR and restriction analysis following standard procedures. Conjugation between *E. coli* WM3064 and *P. khanii* DSM3369 was performed by growing both strains to an OD₆₀₀ of around 0.6. After washing twice with LB medium, cells were mixed in a 1:3 ratio of *E. coli* and *P. khanii*, plated onto LB agar supplemented with diaminopimelic acid (0.3 mM) and incubated at 37 °C for 3 h, followed by overnight incubation at 30 °C. The bacterial lawn was resuspended in LB medium and plated on LB agar with kanamycin (50 µg ml⁻¹) as a serial dilution. Kanamycin-resistant single crossover transconjugants were grown in LB medium to an OD₆₀₀ of approximately 0.6. Then, expression of SacB was induced by adding arabinose (0.2% w/v), followed by 2 h incubation. Subsequently, the culture was plated onto LB agar supplemented with 0.2% (w/v) arabinose and 10% sucrose and incubated at 30 °C for 48 h. Single colonies were picked on LB_{Kan} and LB_{Ara/Suc} agar. Sensitivity to kanamycin indicated plasmid loss and therefore a successful double crossover event. Clones were picked and analysed for BGC loss by PCR using the primers 5'-ATCTCCATCAAAGCGCTACC-3' and 5'-CCGGCTGCAACTCGAAATC-3'. The knockout strain is called *P. khanii* DSM3369 Δ *darABCDE*.

For heterologous expression of the darobactin ABGC in *E. coli* and to complement *P. khanii* DSM3369 Δ *darABCDE*, the expression plasmid pNB03 was used. To avoid issues with the regulation system between the propeptide and the modifying enzymes, all intergenic regions were removed and the genes *dara*–*darE* were expressed streamlined under the control of the arabinose-inducible *araB* promoter.

pNB03 was created by amplification of the p15A ori from pACYC177 (primers 5'-GGTCGACGGATCCCCGGAAATAGCGGAAATGGCTTACG AAC-3' and 5'-CTCTAAGGAGGTATAAAAAGCGGCCGATCCCTT AACGTGAGTTTC-3'); the arabinose expression system and kanamycin-resistance gene of pNB02 (primers 5'-AACGAGCTCC AGCCTACATCAGAAGAACCTCGTAAGAAGGCCA-3' and 5'-TTTTTA TAACCTCCTTAGAGCTCGAATTCC-3'), oriT and the *aac(3)* gene, which confers resistance to apramycin from pJ773⁴³ (primers 5'-ATTCCGGGGA TCCGTCGACC-3' and 5'-TGTAGGCTGGAGCTGCTT-3'). Subsequently, all fragments were gel purified and assembled as described previously. *E. coli* TOP10 cells were transformed with the vector and correct assembly was corroborated. To introduce the *dar* BGC into *P. khanii* DSM3369 Δ *darABCDE*, pNB03 was first linearized using the primers 5'-TCCCTTA ACGTGAGTTTCG-3' and 5'-TTTTATAACCTCCTTAGAGCTCGAA-3', *dara* was then amplified using 5'-GCTCTAAGGAGGTATAAAAATGCATAA TACCTTAATGAAACCGTAAA-3' and 5'-AATAGCATTCTTATGG CTCTCCTTTAAATTCTGGAGCTT-3', and *darB*–*darE* was amplified using 5'-AAAGCTTCCAGGAATTAAAAGGAGGCCATAA ATGAATGCTATT-3' and 5'-CGAAAACCTCACGTTAAGGGATTACGCCGCC ATGGTTGTTTATT-3'. All fragments were gel purified and assembled as described above. The resulting vector pNB03-*darABCDE* was transferred to *E. coli* TOP10 cells and correct assembly was corroborated.

The empty pNB03 and pNB03-*darABCDE* vectors were transferred to *P. khanii* DSM3369 Δ *darABCDE* by triparental conjugation. In brief, conjugation between *P. khanii* DSM3369 Δ *darABCDE*, *E. coli* TOP10 carrying the expression plasmid and *E. coli* ET pUB307, which carried the pUB307 conjugation helper plasmid, was carried out as described above (cell ratio 3:1:1). As *P. khanii* DSM3369 is naturally resistant to carbencillin and the kanamycin resistance of pUB307 lacks the bla promoter, final selection took place on LB agar supplemented with kanamycin and carbencillin. Kanamycin-resistant transconjugants were grown in LB_{Kan}, the plasmid was isolated and the identity verified by PCR. For heterologous expression, the vector pNB03-*darABCDE* was transferred to *E. coli* BW25113 (arabinose non-utilizer) by electroporation.

Subsequently, wild-type *P. khanii* DSM3369, *P. khanii* DSM3369 Δ *darABCDE* and pNB03, *P. khanii* DSM3369 Δ *darABCDE* and pNB03-*darABCDE*, and *E. coli* and pNB03-*darABCDE* were grown in LB or LB_{Kan} supplemented with 0.2% (w/v) arabinose for 5–7 days and analysed by liquid chromatography coupled to mass spectrometry (LC–MS).

Then, the centrifuged culture supernatant was desalted on self-packed C18 columns by washing with 5% acetonitrile, and subsequent elution with 80% acetonitrile in Milli-Q water and 0.1% formic acid. A Dionex UltiMate 3000 HPLC system was coupled to a high-resolution electrospray ionization quadrupole time-of-flight mass spectrometer (QqTOF-ESI-HRMS) from Bruker Daltonics Instruments. Dionex Acclaim 120 C18 (5 µm 4.6 mm × 100 mm) was used for the separation with solvent A (Milli-Q water) and solvent B (100% methanol). The initial concentration of 10% solvent B was maintained for 10 min, followed by a linear gradient to 100% over 30 min. MS parameters were as follows: nebulizer gas, 1.6 bar; gas temperature, 200 °C; gas flow, 8 l min⁻¹; capillary voltage, 4,500 V; endplate offset, 500 V; positive ion mode.

MIC

The MIC was determined by microbroth dilution. Under aerobic conditions, overnight cultures of *E. coli* strains, *P. aeruginosa* strains, *A. baumannii* ATCC 17978, *K. pneumoniae* strains and *S. aureus* HG003, were diluted 1:100 in MHIIB and incubated at 37 °C with aeration at 220 rpm. Exponential cultures (OD₆₀₀ of 0.1–0.9) were diluted to an OD₆₀₀ of 0.001 (approximately 5 × 10⁵ c.f.u. ml⁻¹) in MHIIB and 98 µl aliquots were transferred into round-bottom 96-well plates containing 2 µl of darobactin solutions diluted serially twofold. After overnight incubation at 37 °C, the darobactin MIC was determined as the minimum concentration at which no growth of strains could be detected by eye. For susceptibility testing of *Mycobacterium tuberculosis*, cells were cultured in BD Difco 7H9 base medium supplemented with 10% OADC enrichment (oleic acid, albumin, dextrose and catalase), 0.5% glycerol, 0.2% casamino acids, 0.05% tyloxapol, 80 µg ml⁻¹ lysine and 24 µg ml⁻¹ pantothenate. An exponentially growing culture of strain mc²600 (Δ lys4 Δ panCD) was diluted to an OD₆₀₀ of 0.003 (approximately 5 × 10⁵ cells ml⁻¹) and seeded into 96-well plates containing darobactin dilutions. The plates were incubated for 5 days, then resazurin was added to each well to a final concentration of 2.5 µg ml⁻¹. The plates were incubated for an additional 2 days, at which point the MIC was determined by eye. The MIC against intestinal pathogens and symbionts (*Shigella sonnei*, *Salmonella enterica* Typhimurium LT2, *Moraxella catarrhalis*, *Enterobacter cloacae*, *Bifidobacterium longum*, *Bacteroides fragilis* and *Lactobacillus reuteri* (ATCC 25931, 19585, 25238, 13047, BAA-999, 25285 and 23272, respectively); KLE collection bacteria were isolated from stool under anaerobic conditions and identified by 16S sequencing) was determined under anaerobic conditions (Coy Vinyl Anaerobic chamber, 37 °C, 5% H₂, 10% CO₂, 85% N₂). Overnight cultures grown in brain–heart infusion (BHI) broth, supplemented with 0.5% yeast extract, 0.1% L-cysteine hydrochloride and 15 µg ml⁻¹ haemin (BHI-Ych), were diluted 1:100 in BHI-Ych. The 96-well assay plates were prepared by twofold dilution of darobactin, and included a positive growth control. After 24 h incubation, the MIC was determined. All MIC assays were performed at least in triplicate. The MIC against clinical isolates

(Supplementary Table 1) of *E. coli*, *K. pneumoniae* and *P. aeruginosa* was evaluated by JMI laboratories.

Cytotoxicity

A microplate Alamar blue assay (MABA/resazurin) was used to determine the cytotoxicity of darobactin. Exponentially growing FaDu pharynx squamous cell carcinoma (ATCC HTB-43), HepG2 liver hepatocellular carcinoma (ATCC HB-8065) and red-fluorescent-protein (RFP)-tagged human embryonic kidney 293 (HEK293-RFP; GenTarget SC007) cells, all cultured in Eagle's minimum essential medium supplemented with 10% fetal bovine serum were seeded into a 96-well, flat-bottom, tissue-culture-treated plate (Corning) and incubated at 37 °C with 5% CO₂. After 24 h, the medium was aspirated and replaced with fresh medium containing test compounds (2 µl of a twofold serial dilution in water to 98 µl of medium). After 72 h of incubation at 37 °C with 5% CO₂, resazurin (Acros Organics) was added to each well to a final concentration of 0.15 mM. After 3 h, the absorbances at 544 nm and 590 nm were measured using a BioTek Synergy H1 microplate reader. Experiments were performed in biological triplicate.

Time-dependent killing

An overnight culture of *E. coli* MG1655 was diluted 1:10,000 in MHIIB and incubated at 37 °C for 2 h with aeration at 220 rpm. *E. coli* was treated with 16× MIC antibiotic (64 µg ml⁻¹ darobactin and 64 µg ml⁻¹ ampicillin) and the time at which each antibiotic was added was defined as 0 h. At each time point, 100-µl aliquots were collected and centrifuged at 12,000g for 5 min, pellets washed with 100 µl PBS and resuspended in 100 µl PBS and tenfold serially diluted suspensions were plated onto MHIIA. After overnight cultivation at 37 °C, colonies were counted and c.f.u. ml⁻¹ was calculated. Experiments were performed in biological triplicate.

Resistance studies

E. coli MG1655 cells from an exponential culture were washed in PBS, and subsequently inoculated onto 30 MHIIA plates containing 4× MIC darobactin, at a density of 5×10⁷ c.f.u. per plate. After 2 days of cultivation at 37 °C, plates were examined for colonies, the number of colonies was counted and the colonies were restreaked to test for resistance stability. Subsequently, the colonies were tested by 16S sequencing to ensure that the colonies were *E. coli*. To evolve resistance to darobactin in liquid culture, an overnight culture of *E. coli* MG1655 was diluted 1:100 in 1 ml MHIIB containing 0.5×, 1×, 2× and 4× MIC darobactin and incubated at 37 °C for 24 h with aeration at 220 rpm. The darobactin concentration that inhibited growth of *E. coli* below an OD₆₀₀ of 2.0 was defined as the MIC, and the culture at 0.5× MIC (OD₆₀₀>2) was used to re-inoculate tubes with 0.5×, 1×, 2× and 4× the new MIC at 1:100. This was repeated until cultures were able to grow in 256 µg ml⁻¹ darobactin, and cultures were then maintained in 256 µg ml⁻¹ darobactin until the end of the experiment. Experiments were performed with three independent cultures. For the mutation analysis, more than 3 million paired-end Illumina reads were sequenced for each resistant mutant and mapped to the *E. coli* MG1655 genome (GenBank accession U00096.3) using Geneious v.11.0.4. Single-nucleotide polymorphisms were called using the default parameters, and the generated variant call format (VCF) files were manually filtered to remove calls with a quality score of less than 1,000.

Scanning electron microscopy

E. coli MG1655 samples were prepared as for the time-dependent killing experiments. After washing the cells with PBS, 10 µl cell suspensions were spotted onto Aclar film coated with 0.1% poly-L-lysine. *E. coli* cells were fixed with 2.5% glutaraldehyde in 0.1 M sodium cacodylate containing 0.15% Alcian blue and 0.15% safranin O for 24 h at 4 °C. The samples were washed in 0.1 M sodium cacodylate for 5–10 min, infiltrated with 1% osmium tetroxide for 30 min, washed three times in 0.1 M sodium

cacodylate, and then dehydrated by a graded series of ethanol concentrations (30%, 50%, 70%, 85%, 95% and 100%) for 5–10 min for each concentration. The dehydration step with 100% ethanol was repeated three times. Critical point drying was performed using SAMDRI-PVT-3D (Tousimis) from liquid CO₂. The samples were mounted onto an aluminium sample mount using double-sided conductive-carbon adhesive tape and coated with 5 nm platinum by sputter coating (Cressington 208HR). The samples were imaged with Hitachi S-4800 (Hitachi) at 3.0 kV.

Fluorescence microscopy

E. coli MG1655 was cultured in MHIIB until stationary phase, inoculated into fresh MHIIB at 1:10,000 and grown for 2 h at 37 °C. Cells were concentrated 50-fold in MHIIB, placed on top of a MHIIB–darobactin (64 µg ml⁻¹) 1.5% low-melting agarose pad containing FM4-64 (10 µg ml⁻¹) and Sytox Green (0.5 µM) dyes from Molecular Probes and observed using a ZEISS LSM 710 confocal microscope using a 63× oil-immersion objective lens. The two signals from FM4-64 and Sytox Green were collected after excitation at 488 nm, alongside a differential interference contrast image. The differential interference contrast, FM4-64 and Sytox Green signals were acquired every 30 min at a temperature of 37 °C maintained through a thermostatic chamber. Images were acquired by Zen Software at a resolution of 1,024×1,024 and lane average of 8, and processed with Fiji software⁴⁴. The images shown in Extended Data Fig. 6 were processed using the enhance contrast process, and the HyperStackReg plugin was used to correct for the x-y drift in Supplementary Video 1.

Lipopolysaccharide binding assay

The lipopolysaccharide (LPS) binding assay was performed based on the MIC assay. Aliquots (100 µl) of *E. coli* MG1655 cultures with an OD₆₀₀ of 0.001 and grown in MHIIB were transferred into a 96-well plate containing purified LPS from *E. coli* O55:B5 (0.5–100 µg ml⁻¹; Sigma, L4524) and darobactin or polymyxin B. The antibiotic concentrations that inhibited *E. coli* MG1655 growth were determined in the absence or presence of LPS.

Construction of *bamA* recombinant mutant in *E. coli* MG1655 and ATCC 25922

The linear DNA product comprising the mutated *bamA* gene (1300A>G, 1334A>C and 2113G>A) was amplified by PCR, using the primers *bamA*-recF (5'-ACTATCTGGATCGCGTTATGC-3') and *bamA*-recR (5'-TTCACAGCAGTCTGGATACGAG-3'), and the genomic DNA from *E. coli* darobactin-resistant mutant (strain 3) template. Approximately 500 ng of column-purified mutated *bamA* product was used to transform electrocompetent cells of *E. coli* MG1655-pKD46 to perform λ Red recombination^{41,45}. The subsequent steps have been adapted from the 'Quick and Easy *E. coli* Gene Deletion Kit' (GeneBridges). In brief, 30 µl of an overnight culture of *E. coli* MG1655-pKD46 was used to inoculate a microtube containing 1.4 ml of LB medium complemented with ampicillin (100 µg ml⁻¹). After 2 h of shaking at 30 °C, 0.4% of L-arabinose was added, and the tube was transferred for shaking at 37 °C for 1 h. Cells were washed and concentrated with ice-cold 10% glycerol before electroporation. The recovery step was performed for 3 h at 37 °C with shaking. First selection was performed using resistance to darobactin (32 µg ml⁻¹). Several transformant clones were then restreaked with double selection for resistance to darobactin (32 µg ml⁻¹) and sensitivity to ampicillin (100 µg ml⁻¹, at 30 °C). The *bamA* locus was amplified and the presence of the mutations (1300A>G, 1334A>C and 2113G>A leading to T434A, Q445P and A705T, respectively) was confirmed by sequencing.

For virulence testing, to transfer mutations from strain 3 into *E. coli* ATCC 25922 leading to the triple *bamA* mutant, the same strategy was used. During the manipulation of *E. coli* ATCC 25922 to construct the *bamA* recombinant mutant, two spontaneous *bamA* mutants with

Article

single single-nucleotide polymorphisms were isolated from darobactin-containing plates ($16\text{ }\mu\text{g ml}^{-1}$): 1285G>A, leading to G429R and 1286G>T, leading to G429V.

Transcriptome analysis

For the challenge experiments, 3 ml of *E. coli* BW25113 at an OD_{600} of 0.5, representing mid-log phase, was exposed to $4\text{ }\mu\text{g ml}^{-1}$ darobactin for 15 min, 30 min and 1 h in biological triplicate. After exposure, cells were immediately pelleted at $4\text{ }^\circ\text{C}$ by centrifugation for 2 min at 2,000 rpm in 1-ml aliquots. The supernatants were removed and samples were immediately frozen in liquid nitrogen at $-80\text{ }^\circ\text{C}$ until they were processed for total RNA isolation. Total RNA was extracted by automation using the NucleoMag RNA extraction kit on the EpMotion Robotic liquid handler. For the resulting total RNA, RIN values were obtained to check for RNA quality using the 2200 TapeStation instrument from Agilent Genomics. rRNAs were subtracted from the total RNA to yield only mRNA for library construction using the NEB bacterial rRNA depletion kit at half reactions with a total RNA input maximum of 400 ng. The quality of the rRNA-depleted samples was checked using an Agilent Bioanalyzer with the Agilent Pico chip for RNA detection for less than 0.5% of rRNA remaining in each sample. Then, 2–5 ng of the rRNA-depleted samples was used as the input material to construct each cDNA library for RNA sequencing using the NEBNext Ultra Directional RNA Library prep kit from Illumina. The quality of the resulting libraries was checked using Agilent High Sensitivity DNA chips to ensure proper library size distribution and the absence of small adapters. Libraries were quantified and normalized by qPCR and then sequenced using the NextSeq 500 High Output Kit at 150 cycles producing approximately 9 million, 75-bp, paired-end reads for each library. These reads were mapped to *E. coli* strain BW25113 using clc_assembler v.4.4.2.133896 (CLC Genomics Workbench 11.0). Differential expression was computed using edgeR::exactTest⁴⁶ in R v.3.5.1 with unnormalized gene counts ($n = 4,626$ genes) for each treatment at time t versus the matched control, for $t \in \{15, 30, 60\}$. The gene count matrix was restricted to genes at minimum present in all replicates from one treatment condition resulting in $n = 4,514$ genes. Volcano plots were created using plot_volcano from soothsayer (<https://github.com/jolespin/soothsayer>) in Python v.3.6.6. Directed networks (DiNetwork) were constructed and plotted using NetworkX and Matplotlib Python packages, respectively. Heat maps were generated using seaborn and operon plots were created with Matplotlib.

Two-dimensional thermal proteome profiling

Thermal proteome profiling was performed as previously described^{47,48}. In brief, *E. coli* BW25113 cells were grown aerobically at $37\text{ }^\circ\text{C}$ with shaking until an OD_{578} of approximately 0.7 was reached. For living-cell experiments, darobactin was then added at five different concentrations and incubated for 10 min. For experiments in which protein synthesis was inhibited, cells were treated with 0.2 mg ml^{-1} chloramphenicol for 10 min before addition of darobactin. For lysate experiments, cells were disrupted with five freeze–thaw cycles before darobactin treatment. Aliquots of treated cells or lysates were then heated for 3 min to 10 different temperatures in a PCR machine (Agilent SureCycler 8800). After cell lysis, protein aggregates were removed and the remaining soluble proteins were digested according to a modified SP3 protocol^{49,50}, as previously described⁵¹. Peptides were labelled with TMT10plex (ThermoFisher Scientific), fractionated onto six fractions under high pH conditions and analysed using LC–MS/MS, as previously described⁴⁷. Protein identification and quantification was performed using IsobarQuant⁵² and Mascot 2.4 (Matrix Science) against the *E. coli* Uniprot FASTA (Proteome identifier, UP000000625). Data were analysed with the TPP package for R⁵² followed by a false-discovery rate (FDR)-controlled method for functional analysis of dose–response curves⁵¹. Data are available in Supplementary Table 2.

Cloning, expression and purification of BAM and BAM mutants for nanodiscs

To prepare the BAM mutants, the pJH114 plasmid (a gift from H. Bernstein)³⁷ was used as a template using an Agilent QuikChange Lighting Multi Site-Directed Mutagenesis Kit (Agilent); oligonucleotide sequences are available upon request. The plasmids encoding wild-type BAM (pJH114), with BamE carrying a C-terminal His-tag, and the corresponding BamA mutant genes 1–3 (M1, G429V and G807V; M2, F394V, E435K and G443D; M3, T434A, Q445P and A705T) were cloned under an isopropyl-β-D-thiogalactoside(IPTG) promoter and sequences were confirmed. The primers used for mutation are as below: BAM_mutation1_G429V (5'-TTCAACTTGTATTGGTTAC-3'), BAM_mutation1_G807V (5'-TTAACATCGTAAACCTGG-3'), BAM_mutation2_F394V (5'-CGTCTGGCGTCTTGAAAC-3'), BAM_mutation2_E435K (5'-TACGGTACTAAAGTGGCGTG-3'), BAM_mutation2_G443D (5'-TTCCAGGCTGATGTGCAGCAG-3'), BAM_mutation3_T434A (5'-GGTTACGGTCTGAAAGTGGC-3'), BAM_mutation3_Q445P (5'-GCTGGTGTGCCGAGATAAC-3') and BAM_mutation3_A705T (5'-TCGGATGATACTGTAGGCGG-3'). Plasmids were transformed into BL21(DE3) cells, plated onto LB–carbenicillin agar plates and incubated overnight at $37\text{ }^\circ\text{C}$. After transforming the plasmids into *E. coli* BL21 (DE3), the plasmids were isolated and resequenced. The sequence of M2 and M3 was unchanged, but an additional mutation, T434A, appeared in M1, which we refer to as M1a. This additional mutation matches the T434A mutation in M3, and may have been selected for during cell growth, possibly stabilizing the protein. A 50-ml overnight culture was prepared from a single colony in $2\times$ YT medium supplemented with $100\text{ }\mu\text{g ml}^{-1}$ of ampicillin. The cells were then centrifuged and resuspended in 5 ml of fresh $2\times$ YT medium and then 1 ml was added to five 2-l baffled flasks containing 1 l of $2\times$ YT medium supplemented with $50\text{ }\mu\text{g ml}^{-1}$ of ampicillin. These cultures were grown at $37\text{ }^\circ\text{C}$ until an OD_{600} between 0.8 and 1.0 was reached, after which the cultures were induced with 0.5 mM IPTG and the cells were collected after 3 h. Purification was performed as previously described³⁵. In brief, cells were resuspended in lysis buffer (1× PBS, $10\text{ }\mu\text{g ml}^{-1}$ DNase I, 200 μM PMSF, 2 μM leupeptin and 1.5 nM pepstatin A) and lysed by three passages through an Emulsiflex C-3 homogenizer (Avestin) at 18,000 psi. The lysate was then centrifuged at 6,000g for 20 min and the supernatant was centrifuged at 200,000g for 90 min at $4\text{ }^\circ\text{C}$. The membrane pellets were resuspended into solubilization buffer (50 mM Tris-HCl, pH 7.5, 150 mM NaCl, 0.5% n-dodecyl-β-D-maltoside (DDM) and 37 mM imidazole) using a Dounce homogenizer, and subsequently stirred at $4\text{ }^\circ\text{C}$ for 4 h. Solubilized membranes were then centrifuged at 200,000g for 40 min at $4\text{ }^\circ\text{C}$ to collect the supernatant, which was used for purification using a 5-ml Ni-NTA column on an ÄKTA system (GE Healthcare) using buffer A (25 mM Tris-HCl, pH 7.5, 150 mM NaCl, 0.05% DDM and 37 mM imidazole) and buffer B (25 mM Tris-HCl, pH 7.5, 150 mM NaCl, 0.05% DDM and 1 M imidazole). Fractions containing the protein were pooled, concentrated to 5 ml for size-exclusion chromatography using a 16/60 Sephacryl S-300 HR column at a flow rate of 1.0 ml min^{-1} in 25 mM Tris-HCl, pH 7.5, 150 mM NaCl and 0.6% C₈E₄. The peak fractions were pooled and concentrated as necessary.

Reconstitution of the BAM into nanodiscs

The membrane scaffold protein MSP1E3D1 was expressed and purified from *E. coli* as previously described^{53,54}. BAM was purified by size-exclusion chromatography in 25 mM Tris-HCl, pH 7.5, 150 mM NaCl, 1.0% n-octyl-β-D-glucopyranoside and concentrated to 100 μM. Nanodisc reconstitution was performed in a final volume of 300 μl by adding 20 μM of purified BAM, 100 μM of MSP1E3D1 and 2 mM of *E. coli* polar lipids (Avanti Polar Lipids) to a buffer containing 25 mM Tris-HCl, pH 7.5 and 150 mM NaCl. Bio-beads SM2 (Biorad) were added to the mixture and incubated at $4\text{ }^\circ\text{C}$ overnight. The Bio-beads were spun down and the supernatant was incubated with 300 μl of HisPur Ni-NTA

Resin (ThermoFisher Scientific) for 30 min at 4 °C. The BAM-inserted nanodiscs were then eluted from the Ni-NTA resin with 25 mM Tris-HCl, pH 7.5, 150 mM NaCl and 400 mM imidazole. The elution was then loaded onto a Superdex 200 Increase 10/300 GL column (GE Healthcare) in 25 mM Tris-HCl, pH 7.5 and 150 mM NaCl. The peak fractions were then pooled and concentrated to 40 µM.

BAM folding assay

OmpT and SurA (periplasmic chaperone) were expressed and purified from *E. coli* as previously reported^{55,56}. Solution 1 contained 0.4 µM BAM-nanodiscs, 0.6 µM of the fluorogenic peptide (Abz-Ala-Arg-Arg-Ala-Tyr(NO₂)-NH₂), and 0.1 mg ml⁻¹ LPS in 25 µl of 20 mM Tris-HCl, pH 6.5. Empty nanodiscs were used as a negative control. Solution 2 contained 20 µM urea-denatured OmpT with 140 µM SurA in 25 µl of 20 mM Tris-HCl, pH 6.5. To initiate the BAM folding reaction, solution 2 was incubated at room temperature for 10 min and then mixed with solution 1. Darobactin was added to solution 1 and incubated for 10 min before being mixed with solution 2. The fluorescence signal was monitored at 430 nm (excitation at 325 nm) using a SpectraMax M2e fluorescent plate reader (Molecular Devices) for 60 min with readings every 8 s. Data were then analysed and plotted using the online IC₅₀ Calculator tool (AAT Bioquest) and GraphPad Prism v8.2.

Isothermal titration calorimetry

All isothermal titration calorimetry (ITC) experiments were carried out at 25 °C with the NanoITC microcalorimeter (TA Instruments) in duplicate. BAM (300 µl) at a concentration of 20 µM in 1× PBS supplemented with 0.05% DDM was placed in the sample cell, and the ligand (darobactin or the linear peptide) with a concentration of 200 µM in the syringe (50 µl) was injected in 20 successive injections with a spacing of 300 s and a stirring rate of 300 rpm. Control experiments in the absence of BAM were performed under identical conditions to determine the heat signal attributable to only the injection of the ligand to the buffer. The resulting data were analysed and fit to the independent binding model using the NanoAnalyze software package (TA Instruments).

Sample preparation of BamA-β in lauryldimethylamine-N-oxide micelles for NMR

The protein construct comprising the β-barrel of *E. coli* BamA (residues 426–810, C690S, C700S; termed BamA-β) was established previously and sample production followed published protocols²¹. In brief, protein expression was carried out in *E. coli* BL21 (DE3) Lemo cells in M9 medium containing ¹⁵NH₄Cl and D₂O. Once the OD₆₀₀ reached 0.8, expression into inclusion bodies was induced by 1 mM IPTG at 37 °C for 12 h. The collected cells were resuspended in buffer A (20 mM Tris pH 8.0 and 300 mM NaCl) and lysed by sonication. Inclusion bodies were collected by centrifugation at 30,000g for 1 h and solubilized into 20 mM Tris pH 8.0 and 6 M guanidinium hydrochloride for 2 h. The solubilized sample was loaded onto Ni-NTA beads preequilibrated with buffer A supplemented with 6 M guanidium hydrochloride. The protein was eluted with buffer A, containing 6 M guanidium hydrochloride and 200 mM imidazole. Refolding was carried out in 20 mM Tris, 150 mM NaCl, pH 8.0 and 0.5% w/v lauryldimethylamine-N-oxide (LDAO) at 4 °C. The refolded sample was dialysed in 20 mM Tris, pH 8.0 overnight. Afterwards, folded BamA-β was purified by ion exchange in 20 mM Tris pH 8.0, 0.1% LDAO and the protein was eluted with a linear gradient of 0.5 M NaCl. Finally, BamA-β was loaded onto a size-exclusion chromatography column (HiLoad 16/600 Superdex 200 pg, GE Healthcare) in 20 mM phosphate buffer pH 7.5, 150 mM NaCl and 0.1% LDAO yielding a monomeric sample.

Solution NMR spectroscopy

A sample was concentrated to an initial protein concentration of 250 µM. Darobactin was added stepwise from a stock solution to 0.5:1-, 1:1- and 2:1-fold stoichiometry darobactin:BamA-β. At each

titration step, a two-dimensional [¹⁵N, ¹H]-TROSY experiment with 64 transients was recorded on a 700-MHz Bruker spectrometer equipped with a cryogenic probe at 37 °C. Then, 1,024 and 128 complex points were acquired in the direct and indirect dimension, respectively, and zero-filled to 2,048 and 256 points during processing. As a control experiment, a linear scrambled peptide WNKWSFS was synthesized, and added at 230 µM to BamA-β. The NMR spectra of 0:1-, 1:1- and 2:1-fold stoichiometry with darobactin:BamA-β, and 0:1 and 1:1 with the peptide WNKWSFS are provided as raw data (Supplementary Data 1). From these, spectra shown in Fig. 3c and Extended Data Fig. 5i, j have been produced. The data format is readable using the standard NMR software TOPSPIN 3.6.2. An upper limit estimate for the dissociation constant K_d was obtained from a quantification of the relative amounts of ligand-free and ligand-bound BamA from NMR signal intensities under consideration of the spectral noise (Fig. 3c).

Animal studies

All animal studies were performed at Northeastern University, approved by Northeastern IACUC, and were performed according to institutional animal care and use policies. Experiments were not randomized nor blinded, as it was not deemed necessary. Female CD-1 mice (20–25 g, experimentally naive, 6 weeks old) from Charles River were used for all studies.

Virulence model. *E. coli* ATCC 25922, both wild-type and with *bamA* mutations leading to darobactin resistance (see ‘Construction of *bamA* recombinant mutant in *E. coli* MG1655 and ATCC 25922’), were tested in an acute infection model. An overnight culture (OD₆₀₀ of 2.0) of *E. coli* was diluted 1:10 in MHIB. Mice were infected with 0.1 ml of bacterial suspension, 2 × 10⁷ c.f.u. for all strains (determined by plate counts), and monitored for survival. At 24 h after infection, mice were euthanized by CO₂ asphyxiation, unless the animals were already dead. The spleen and a piece of liver (lower lobe) were aseptically removed, weighed, homogenized, serially diluted and plated on LB agar and MacConkey agar for c.f.u. titres.

Pharmacokinetic analysis. Mice were injected intraperitoneally with a single dose of 50 mg kg⁻¹ darobactin, in 10% PEG-200. Blood samples were collected from n = 3 mice at each time point (0.25, 0.5, 1, 2, 3, 5, 8 and 24 h) via a tail snip, 10 µl of blood was diluted into 90 µl of chilled saline, and subsequently centrifuged at 1,000g for 5 min. The diluted plasma was decanted into a fresh tube and kept at -80 °C. Blood was collected from an untreated mouse and diluted in saline, and a standard curve generated by addition of known concentrations (0.1, 1, 10, and 100 µg ml⁻¹) of darobactin to decanted supernatant. All of the samples were run on LC-MS to determine the concentration of the compound in the blood. An Agilent 1260 Infinity liquid chromatography system and 6460 triple quadrupole (QqQ) system (Agilent Technologies) were used to quantify darobactin. A Thermo Scientific Accucore C18 column (50 mm × 2.1 mm, 2.6 µm) was used for the separation with a flow rate of 200 µl min⁻¹ with solvent A (0.1% (v/v) formic acid in Milli-Q water) and solvent B (0.1% (v/v) formic acid in acetonitrile). The initial concentration of 2% solvent B was maintained for 2 min, followed by a linear gradient to 70% over 10 min. MS parameters were as follows: gas temperature, 300 °C; gas flow, 7 l min⁻¹; capillary voltage, 3,500 V; fragmentor voltage, 100 V; scan type, MRM; transition parent ion 483.8 to product ions 211.3, 160.1, 120.1 and 103.1 with collision energy 42, 46, 50 and 94 V, respectively. MassHunter qualitative and quantitative analysis B.05 (Agilent Technologies) was used to quantify the darobactin peaks.

Septicaemia model. Darobactin was tested in a septicaemia protection model against *E. coli*, wild type (ATCC 25922) or multidrug-resistant (AR350, CDC), *P. aeruginosa*, wild-type PAO1 and a spontaneous polymyxin-resistant mutant (*pmrB* 523C>T mutation), and *KPC K. pneumoniae* (ATCC BAA1705). Mice were infected with 0.5 ml of bacterial

Article

suspension in BHI with 5% mucin (1×10^6 cells for *E. coli* and *K. pneumoniae*, 8×10^6 and 4×10^6 cells for *P. aeruginosa* wild-type and *pmrB* mutant strains, respectively) via intraperitoneal injection. This dose achieves >90% mortality within 24 h after infection. At 1 h after infection, mice received treatments with darobactin from 50 mg kg^{-1} to 1 mg kg^{-1} administered by intraperitoneal injection. Infection control mice were treated with 20 mg kg^{-1} gentamicin as positive controls and the vehicle alone as a negative control. Survival was monitored for 7 days.

Thigh infection model. Darobactin was tested in a neutropenic thigh infection model against multidrug-resistant *E. coli* AR350 (CDC). Mice were rendered neutropenic through cyclophosphamide injections 4 days (150 mg kg^{-1}) and 1 day (100 mg kg^{-1}) before infection. An overnight culture (OD_{600} of 2.0) of *E. coli* was diluted 1:1,000. Mice were infected with $100 \mu\text{l}$ of the prepared inoculum into the right thigh with the actual inoculum being 10^4 – 10^5 c.f.u. (determined by plate counts), and one group of mice was euthanized and the thighs collected and processed for time 0 counts. At 2 h after infection, mice received treatments with darobactin at 25 mg kg^{-1} (given as 3 doses every 6 h) or 50 mg kg^{-1} (given once) or gentamicin at 20 mg kg^{-1} (one experiment, $n=4$) or 50 mg kg^{-1} (two experiments, $n=5$ each) as a positive control, administered by intraperitoneal injection. At the time of treatment, one group of infected mice was euthanized, and thighs were collected and processed for c.f.u. At 26 h after infection, mice were euthanized via CO_2 asphyxiation. The right quadriceps muscles were aseptically removed, weighed, homogenized, serially diluted and plated on MHIA for c.f.u. titres. This experiment was repeated on three separate occasions with one experiment containing $n=4$ and two experiments containing $n=5$ mice per group.

Statistics

Confidence intervals for IC_{50} values in the BAM folding assay were calculated by GraphPad Prism v.8.2 using nonlinear regression [inhibitor] versus response, constraining the bottom to 0. Significance in transcriptome data for a differentially expressed gene was determined by $|\log_2(\text{fold change (FC)})| \geq 2$ and FDR-adjusted $P < 0.001$, differential expression was computed using the edgeR::exactTest⁴⁶ in R v.3.5.1 with unnormalized gene counts ($n=4,626$ genes) for each treatment at time t versus matched control. For thermal proteome profiling, significant hits (FDR-adjusted $P < 1\%$) were calculated as previously described⁵¹.

Reporting summary

Further information on research design is available in the Nature Research Reporting Summary linked to this paper.

Data availability

All data supporting the findings of this study are available within the paper and its Supplementary Information or have been deposited to the indicated databases. The genome of *P. khanii* HGB1456 has been deposited to GenBank with accession number WHZZ000000000. The transcriptomic dataset (Extended Data Fig. 7) has been deposited to NCBI Sequence Read Archive with identifier PRJNA530781. The mass spectrometry proteomics (Extended Data Fig. 8 and Supplementary Table 2) data have been deposited to the ProteomeXchange Consortium via the PRIDE partner repository with the dataset identifier PXD013319. Source Data for Figs. 2c, 4 and Extended Data Figs. 5b, 9 are provided with the paper. All other data are available from the corresponding author.

38. Antipov, D., Korobeynikov, A., McLean, J. S. & Pevzner, P. A. hybridSPADEs: an algorithm for hybrid assembly of short and long reads. *Bioinformatics* **32**, 1009–1015 (2016).
39. Blin, K. et al. antiSMASH 4.0—improvements in chemistry prediction and gene cluster boundary identification. *Nucleic Acids Res.* **45**, W36–W41 (2017).
40. Lassak, J., Henche, A. L., Binnenkade, L. & Thormann, K. M. ArcS, the cognate sensor kinase in an atypical Arc system of *Shewanella oneidensis* MR-1. *Appl. Environ. Microbiol.* **76**, 3263–3274 (2010).
41. Datsenko, K. A. & Wanner, B. L. One-step inactivation of chromosomal genes in *Escherichia coli* K-12 using PCR products. *Proc. Natl. Acad. Sci. USA* **97**, 6640–6645 (2000).
42. Tang, X. et al. Identification of thiotetronic acid antibiotic biosynthetic pathways by target-directed genome mining. *ACS Chem. Biol.* **10**, 2841–2849 (2015).
43. Gust, B., Challis, G. L., Fowler, K., Kieser, T. & Chater, K. F. PCR-targeted *Streptomyces* gene replacement identifies a protein domain needed for biosynthesis of the sesquiterpene soil odor geosmin. *Proc. Natl. Acad. Sci. USA* **100**, 1541–1546 (2003).
44. Schindelin, J. et al. Fiji: an open-source platform for biological-image analysis. *Nat. Methods* **9**, 676–682 (2012).
45. Murphy, K. C. & Campellone, K. G. Lambda Red-mediated recombinogenic engineering of enterohemorrhagic and enteropathogenic *E. coli*. *BMC Mol. Biol.* **4**, 11 (2003).
46. Robinson, M. D., McCarthy, D. J. & Smyth, G. K. edgeR: a Bioconductor package for differential expression analysis of digital gene expression data. *Bioinformatics* **26**, 139–140 (2010).
47. Mateus, A. et al. Thermal proteome profiling in bacteria: probing protein state in vivo. *Mol. Syst. Biol.* **14**, e8242 (2018).
48. Becher, I. et al. Thermal profiling reveals phenylalanine hydroxylase as an off-target of panobinostat. *Nat. Chem. Biol.* **12**, 908–910 (2016).
49. Hughes, C. S. et al. Ultrasensitive proteome analysis using paramagnetic bead technology. *Mol. Syst. Biol.* **10**, 757 (2014).
50. Hughes, C. S. et al. Single-pot, solid-phase-enhanced sample preparation for proteomics experiments. *Nat. Protoc.* **14**, 68–85 (2019).
51. Sridharan, S. et al. Proteome-wide solubility and thermal stability profiling reveals distinct regulatory roles for ATP. *Nat. Commun.* **10**, 1155 (2019).
52. Franken, H. et al. Thermal proteome profiling for unbiased identification of direct and indirect drug targets using multiplexed quantitative mass spectrometry. *Nat. Protoc.* **10**, 1567–1593 (2015).
53. Alvarez, F. J. D., Orelle, C. & Davidson, A. L. Functional reconstitution of an ABC transporter in nanodiscs for use in electron paramagnetic resonance spectroscopy. *J. Am. Chem. Soc.* **132**, 9513–9515 (2010).
54. Ritchie, T. K. et al. Chapter 11 - Reconstitution of membrane proteins in phospholipid bilayer nanodiscs. *Methods Enzymol.* **464**, 211–231 (2009).
55. Roman-Hernandez, G., Peterson, J. H. & Bernstein, H. D. Reconstitution of bacterial autotransporter assembly using purified components. *eLife* **3**, e04234 (2014).
56. Hagan, C. L., Kim, S. & Kahne, D. Reconstitution of outer membrane protein assembly from purified components. *Science* **328**, 890–892 (2010).

Acknowledgements This work was supported by NIH grant P01 AI118687 to K.L. and K.E.N. A. Mateus was supported by a fellowship from the EMBL Interdisciplinary Postdoc (EI3POD) Programme under Marie Skłodowska-Curie Actions COFUND (grant number 664726). S.H. was supported by the Swiss National Science Foundation via the NFP 72 (407240_167125). N.N. was supported by NIH grants GM127896 and GM127884. We thank H. Goodrich-Blair for providing strains of *Photobacterium* and *Xenorhabdus*; M. Kagan for help with isolating darobactin; the Northeastern University Barnett Institute MS Core Facility for access to its LC–MS resources; D. Baldissari from Bruker Biospin Corporation for recording some of the NMR data of darobactin; N. Kurzawa for the help with the analysis of thermal proteome profiling data; W. Fowle for assistance with scanning electron microscopy experiments; Y. Su for assistance with the ITC experiments; and R. Machado for help with taxonomy of *Photobacterium*.

Author contributions K.L. designed the study, analysed results and wrote the paper. Y.I. identified darobactin, designed the study and analysed results. K.J.M. designed the animal study, wrote the paper and analysed results. A.I. performed mass spectrometry and, with M.M., isolated darobactin. Q.F.-G., C.H., X.M., J.J.G. and A. Makriyannis identified the structure of darobactin. A.D. provided logistical support for the study. S.M. performed microscopy studies and analysed data. M.C. and M.G. performed susceptibility studies. S.N. performed animal studies. T.F.S., R.G., N.B., Z.G.W. and L.L.-O. identified darobactin BGCs and generated the knockout and heterologous expression strains. H.K. performed the NMR studies of BamA. S.H. designed and analysed the NMR studies and wrote the paper. R.W. performed the BAM nanodisc studies. N.N. designed and analysed the BAM nanodisc studies and wrote the paper. A.T., M.M.S. and A. Mateus performed the proteomics study and analysed data. K.E.N., J.L.E. and A.O. performed the transcriptome study and analysed data.

Competing interests The authors declare no competing interests.

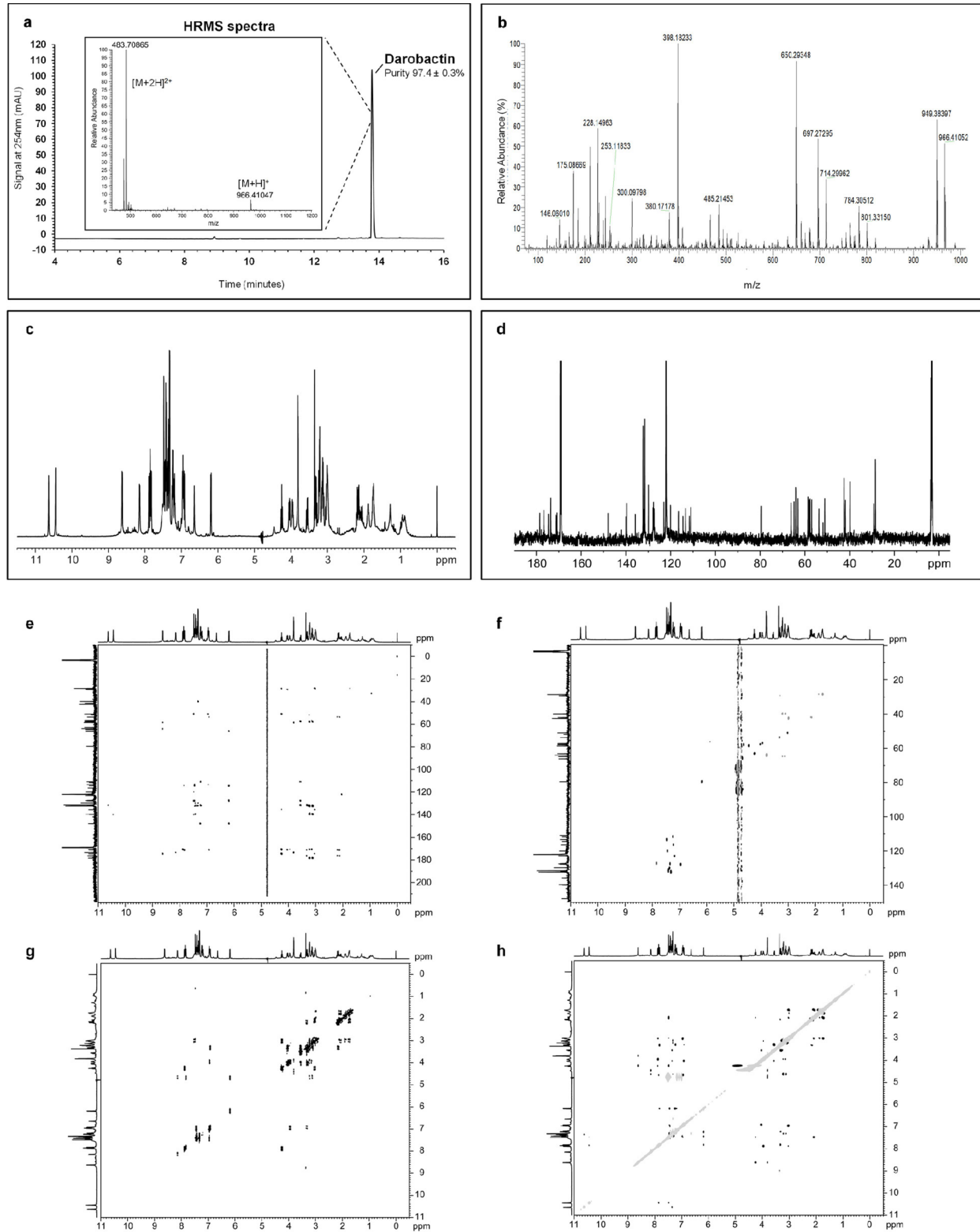
Additional information

Supplementary information is available for this paper at <https://doi.org/10.1038/s41586-019-1791-1>.

Correspondence and requests for materials should be addressed to K.L.

Peer review information *Nature* thanks Eric Brown, Tilmann Weber and the other, anonymous, reviewer(s) for their contribution to the peer review of this work.

Reprints and permissions information is available at <http://www.nature.com/reprints>.

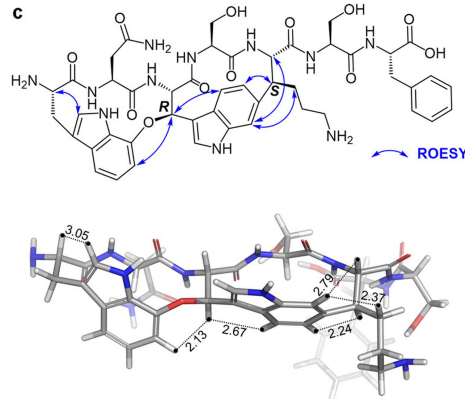
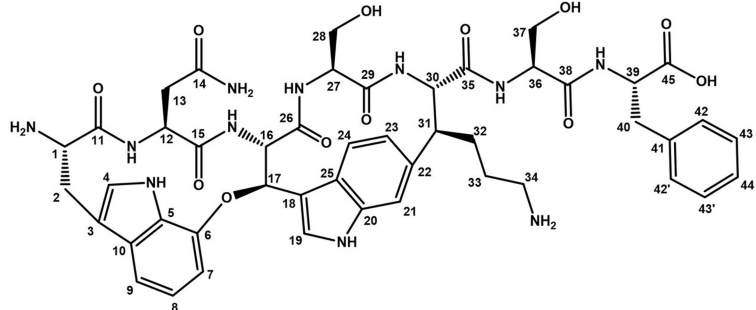


Extended Data Fig. 1 | Structural determination of darobactin. **a**, HPLC chromatogram of darobactin. Inset, high-resolution mass spectra (HRMS) of darobactin showing a peak at m/z 966.41047, which corresponds to the $[M + H]^+$ ion and another at m/z 483.70865, which corresponds to $[M + 2H]^{2+}$ ion.

b, Higher-energy collisional dissociation–MS/MS spectra of darobactin. **c**, ^1H NMR spectrum of darobactin. **d**, ^{13}C NMR spectrum. **e**, ^1H - ^{13}C HMBC NMR spectrum. **f**, ^1H - ^{13}C HSQC NMR spectrum. **g**, COSY NMR spectrum. **h**, ROESY NMR spectrum.

a

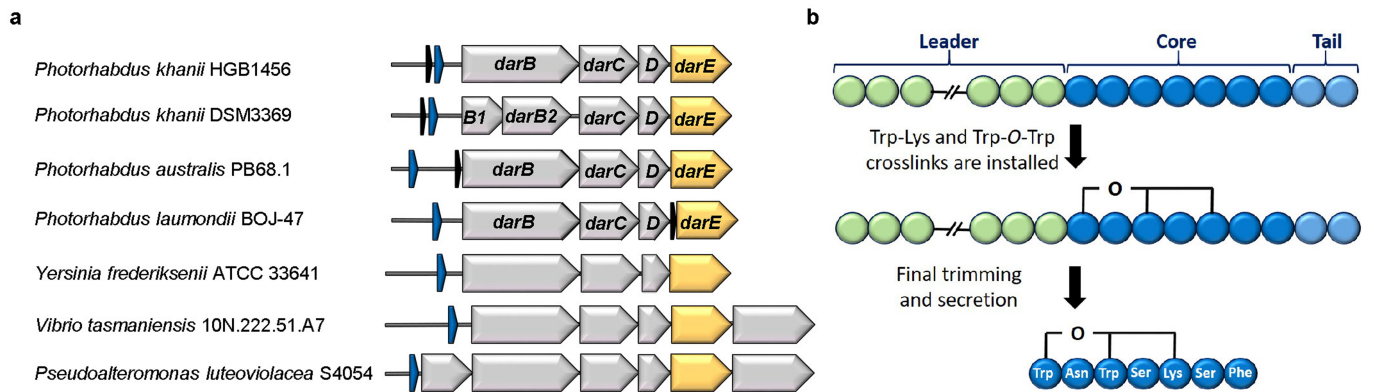
¹ H, ¹³ C and ¹⁵ N NMR chemical shifts (ppm) for Darobactin					
Position	$\delta_{\text{C}} / \delta_{\text{N}}$	δ_{H} (mult., J in Hz)	Position	$\delta_{\text{C}} / \delta_{\text{N}}$	δ_{H} (mult., J in Hz)
1	57.6	4.04 (1H, dd, 11.2, 7.7)	24	120.0	7.45 (1H, d, m)
1-NH ₂	-	exchanged	25	127.8	-
2	29.2	3.55 (1H, dd, 14.1, 7.6) 3.30 (1H, dd, m)	26	170.7	-
3	111.0	-	26-NH	121.9	6.95 (1H, d, m)
4	127.6	7.35 (1H, br s)	27	56.9	3.95 (1H, m)
4-NH	128.8	10.63 (1H, br s)	28	64.8	3.22 (1H, dd, m)
5	131.8 [‡]	-	29	170.9	-
6	147.9	-	29-NH	127.0	7.88 (1H, d, 10.7)
7	111.6	7.24 (1H, d, 7.7)	30	63.0	4.25 (1H, t, 10.9)
8	123.0	7.18 (1H, t, 7.7)	31	51.0	3.03 (1H, m)
9	116.5	7.22 (1H, d, 7.7)	32	28.5	2.08 (1H, m)
10	131.8 [‡]	-	33	28.5	1.88 (1H, m)
11	171.1	-			1.74 (1H, m)
11-NH	124.5	6.92 (1H, d, 8.1)	34	42.4	2.99 (1H, m)
12	53.7	3.33 (1H, m)	34-NH ₂	-	7.51 (2H, v br s)
13	41.9	2.19 (1H, dd, 13.9, 7.2) 2.13 (1H, dd, 13.9, 7.2)	35	174.6	-
14	176.6	-	35-NH	122.8	8.62 (1H, d, 7.3)
14-NH ₂	113.8	7.31 (1H, br s) 6.64 (1H, br s)	36	58.5	4.46 (1H, m)
15	171.3	-	37	64.0	3.80 (2H, d, 5.5)
15-NH	123.0	7.83 (1H, d, 9.8)	38	173.5	-
16	66.1	4.69 (1H, dd, 9.1, 10.2) [†]	38-NH	123.6	8.14 (1H, d, 7.4)
17	79.5	6.18 (1H, d, 9.1)	39	57.9	4.64 (1H, dt, 7.7, 5.9) [†]
18	114.5	-	40	39.8	3.11 (1H, dd, m)
19	127.4	7.85 (1H, br s)	41	139.6	3.22 (1H, dd, m)
20	139.9	-	42, 42'	132.3	7.32 (2H, d, m)
20-NH	133.2	10.44 (1H, br s)	43, 43'	131.5	7.42 (2H, t, 7.49)
21	113.3	7.48 (1H, br s)	44	129.9	7.37 (1H, t, 7.08)
22	135.7	-	45	178.4	-
23	127.7	6.96 (1H, d, m)			

b

Extended Data Fig. 2 | NMR assignments of darobactin. **a**, ¹H, ¹³C and ¹⁵N NMR chemical shifts (ppm) for darobactin. ¹Owing to overlap with a residual water peak at 4.6 ppm, the multiplicity and coupling values were from a different ¹H NMR spectrum of darobactin in water:deuterated acetonitrile (2:1, v/v). ²Two

partially overlapping peaks were observed at 131.79 ppm and 131.83 ppm.

b, Structure of darobactin with numbering for NMR assignments. **c**, Key ROESY correlations (top) and three-dimensional model of darobactin (bottom).



c

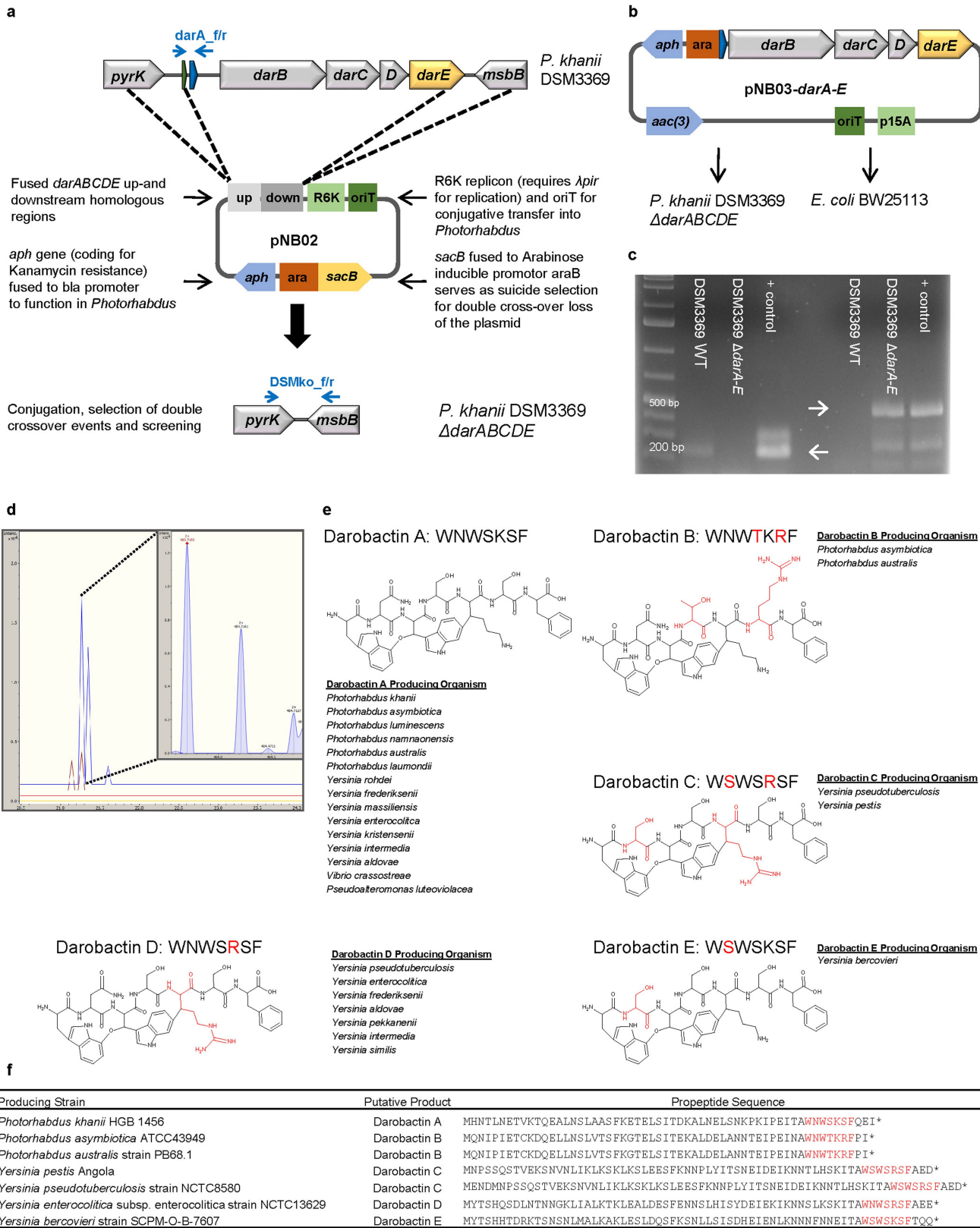
<i>Photorhabdus khanii</i> HGB1456	MHNTLNETVKTQEALNSLAASFKETELSI TDKALNELSNKPKIPEITA WNWSKSF QEI*
<i>Photorhabdus khanii</i> DSM3369	MHNTLNETVKTQEALNSLAASFKETELSI TDKALNELSNKPKIPEITA WNWSKSF QEI*
<i>Photorhabdus australis</i> PB68.1	MQNTLVETCKTQEALNSLAASFKETELSI TEKALNELSSKPKIPEITA WNWSKSF QEI*
<i>Photorhabdus laumontii</i> BOJ-47	MHNTSI INCTTQEALNSLAASFKDTELSITERALDELNNKPKIPEITA WNWSKSF QEI*
<i>Yersinia frederiksenii</i> ATCC 33641	MHTSHQPDKKTGNTHLITLTKLESLEESFKNSSLISINDHEIESLNKNSDSDNKITA WNWSKSFTQQ*
<i>Vibrio tasmaniensis</i> 10N.222.51.A7	MIIVEKEKVSI SERLDALMSSFSEMNL ELTKFDQE VNSINIAPPITA WNWSKSF *
<i>Pseudoalteromonas luteoviolacea</i> S4054	MIVEAPKEKVSI SEKLDALKSSFSNQTLNIANVDQARVDSISVAPPITA WNWSKSFEK*

Extended Data Fig. 3 | BGC of darobactin in selected bacterial strains.

a, The BGC consists of the structural gene *darA* (coloured in blue), *darBCD* (transporter encoding genes; grey) and *darE* (a radical SAM enzyme; orange). In addition, a *relE*-like gene (black) open-reading frame is co-located with the BGC at different positions in different species. The BGC can be detected in most *Photorhabdus* strains in a conserved genetic region. In addition, homologous BGCs (related genes show the identical colour code) can be found in *Yersinia*,

Vibrio and *Pseudoalteromonas* strains. **b**, Biosynthetic hypothesis. The propeptide encoded by *darA* consists of 58 amino acids. The crosslinks are installed on the linear propeptide by DarE. In a next step, the leader and tail regions are cleaved off and darobactin is secreted by the ABC transporter DarBCD. **c**, The amino acid sequence of the propeptide from selected bacterial strains. The darobactin core peptide is highlighted in bold and the amino acids involved in the crosslinking in bold red. The asterisk indicates the stop codon.

Article

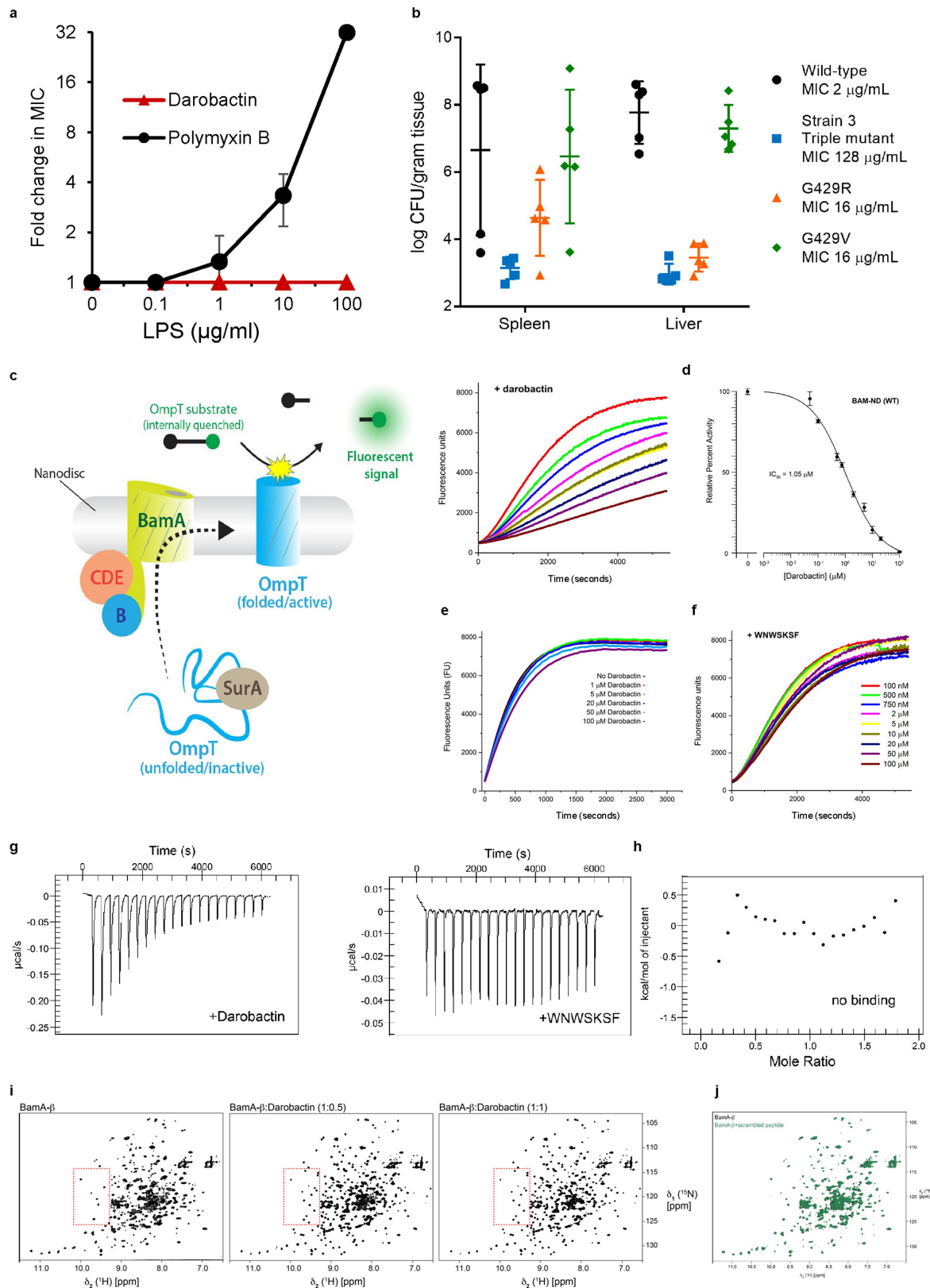


Extended Data Fig. 4 | Darobactin knockout strain and heterologous expression, and putative structures and producers of darobactin A–E.

a, Schematic of the double crossover knockout vector pNB02 and the targeted genomic region. **b**, Schematic of the darobactin BGC expression plasmid. **c**, Test PCRs on *P. khanii* DSM3369 Δ *darABCDE*, showing the loss of the darobactin BGC. Left, amplification of *darA* (primers darA_f/r) results in a 177-bp fragment in the wild-type (WT) strain and in no fragment in the mutant. Right, after loss of pNB02 (indicated by sensitivity to kanamycin), amplification of a 450-bp fragment if the BGC is deleted (primers DSMko_f/r) occurs. Positive controls include pNB03-*darA-E* and pNB02. Primer positions are indicated in blue in **a**. The raw DNA gel is provided in Supplementary Fig. 1. **d**, LC–MS-extracted ion chromatogram at $m/z = 483.7089 \pm 0.001$. Yellow,

P. khanii DSM3369 Δ *darABCDE* and pNB03; red, *P. khanii* DSM3369 Δ *darABCDE* and pNB03-*darA-E*; brown, *E. coli* BW25113 and pNB03-*darA-E*; blue, *P. khanii* DSM3369 wild type. Inset, HRMS spectrum of the ion peak showing the double charged $[M + 2H]^{2+}$ ion that corresponds to darobactin. **e**, **f**, Data are representative of at least three independent biological replicates. **e**, Putative darobactin analogues B–E were drawn based on the amino acid sequence that is present in the darobactin BGC. The proposed darobactin-producing organisms were identified by a BLASTp search of the seven-amino-acid sequence of darobactin A, confirming the presence of *darBCDE* downstream of the propeptide. Amino acid changes from darobactin A are highlighted in red. **f**, The propeptide sequence of the various darobactin analogues.

Article



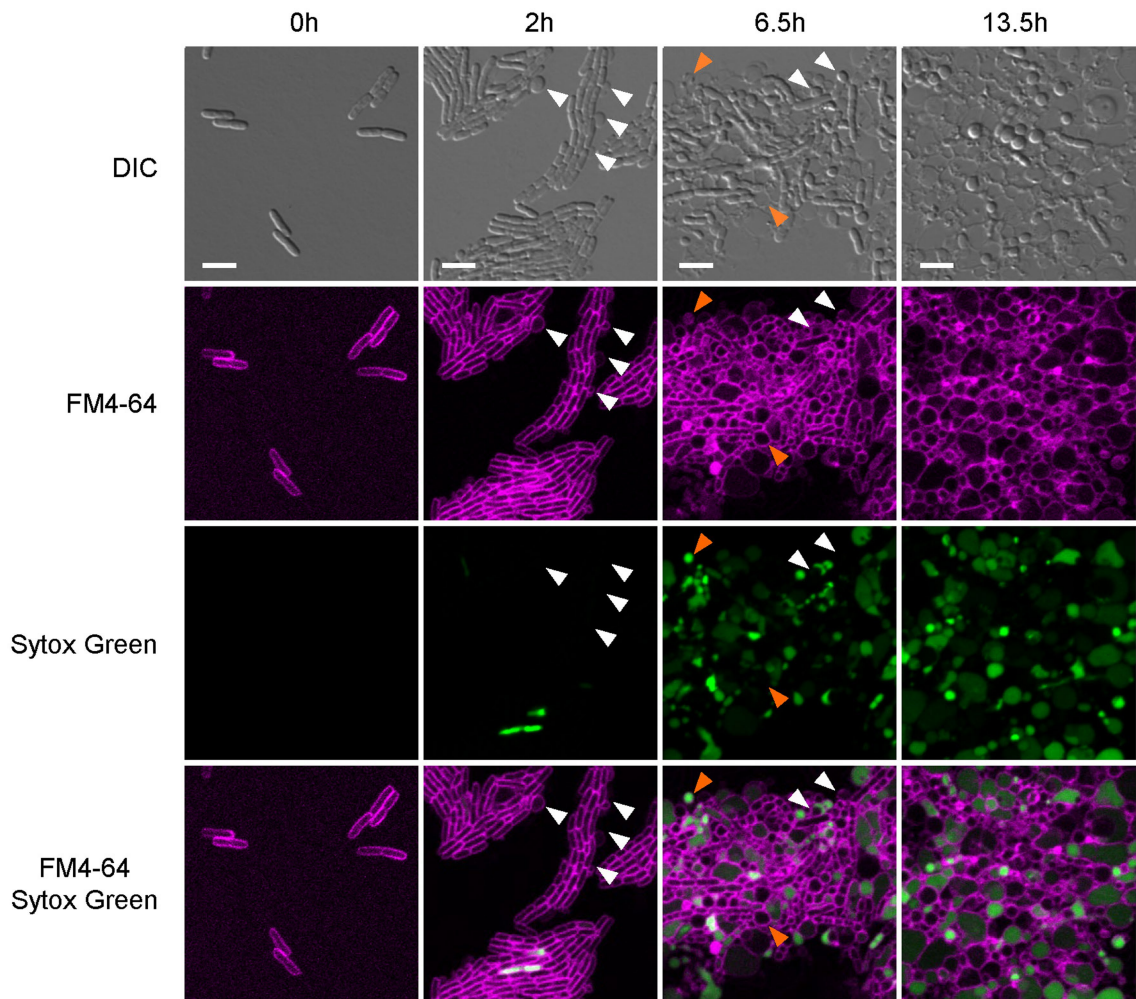
Extended Data Fig. 5 | See next page for caption.

Extended Data Fig. 5 | Darobactin mechanism of action and resistance studies.

a, Darobactin and polymyxin B MIC studies against *E. coli* MG1655 were performed in the presence of LPS. Addition of LPS antagonized polymyxin activity, but not darobactin activity. Data are mean \pm s.d. of triplicate experiments. **b**, Groups of five mice were infected intraperitoneally with 10^7 *E. coli* ATCC 25922, and subsequently euthanized at 24 h (if not already dead), after which the livers and spleens collected, homogenized and plated for c.f.u. analysis. Wild-type *E. coli* caused 60% death and showed high c.f.u. burdens in liver and spleen. All three darobactin-resistant *bamA* mutant strains had reduced virulence, with 100% survival in all groups at 24 h. The burden of bacteria of the triple *bamA* mutant was close to the limit of detection in organs, the G429R-expressing mutant was found at low but detectable levels, whereas the G429V-expressing mutant was found at relatively high loads in the organs. $n=5$. Data are mean \pm s.d. **c**, Schematic of the BAM activity assay in which BAM (BamA–E) was first inserted into lipid nanodiscs. Unfolded OmpT, along with the periplasmic chaperone SurA, was then mixed with the BAM–nanodiscs, and BAM folds OmpT into the nanodisc. OmpT, a protease, cleaves an internally quenched peptide, which produces a fluorescent signal. **d**, BAM–nanodisc assays performed in the presence of increasing concentrations of darobactin (left). The results show that darobactin is able to specifically inhibit BAM–nanodisc activity in a dose-dependent manner. These data were then normalized against the ‘no darobactin’ sample and the highest concentration of darobactin and plotted, and an IC_{50} was calculated using the online IC_{50} calculator tool (AAT Bioquest) (right). ND, nanodisc. $n=3$ biologically independent experiments. Data are mean \pm s.d. **e**, As a control to the BAM–nanodisc assays, we prepared OmpT–nanodiscs and assayed OmpT–nanodisc activity in the presence of increasing concentrations of darobactin. To prepare

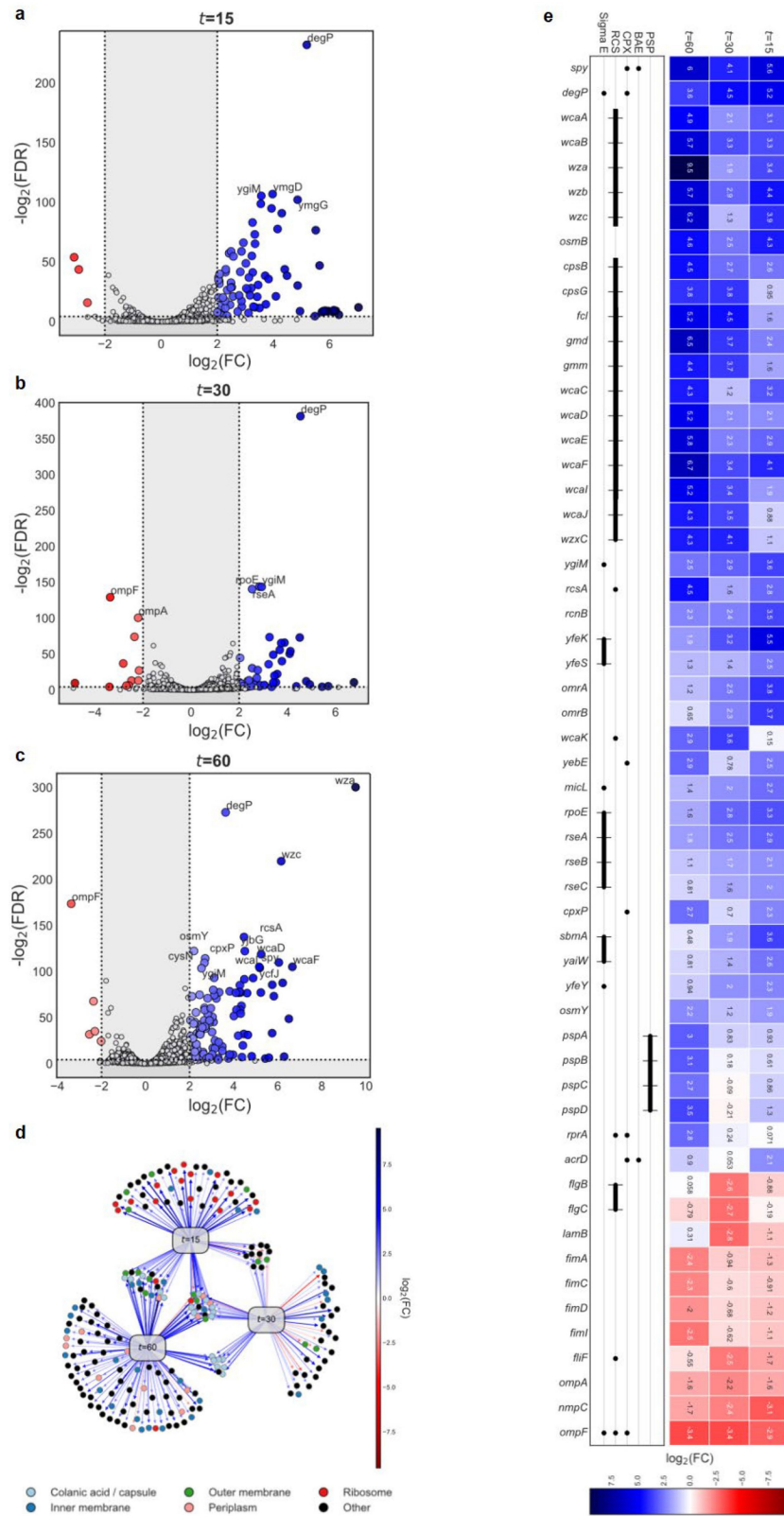
the OmpT–nanodiscs, we first expressed OmpT as inclusion bodies and then refolded the protein using previously reported methods^{55,56}. We then incorporated OmpT into nanodiscs using the same methods as described for BAM. The assays were performed using 0.4 μ M of OmpT–nanodiscs. The results show that darobactin has almost no effect on OmpT–nanodisc activity, thus confirming that darobactin does not affect OmpT activity itself or disrupting the nanodiscs themselves. A representative plot is shown from a triplicate experiment. **f**, The WNWSKSF peptide does not inhibit BAM–nanodiscs. As a control to darobactin, the BAM–nanodisc assays were performed in the presence of increasing concentrations of a linear peptide WNWSKSF. The results show that the WNWSKSF peptide has only minimal effects on BAM–nanodisc activity, even at the highest concentrations. A representative plot is shown from a triplicate experiment. **g, h**, Specific binding of darobactin to BamA/BAM. Mole ratio is the protein:ligand ratio. **g**, Plot of ITC experiments of wild-type BAM titrated with darobactin. $K_d=1.2\text{ }\mu\text{M}$, $N=0.52$, $\Delta H=-25\text{ kcal mol}^{-1}$ and $\Delta S=-56\text{ cal mol}^{-1}\text{ K}^{-1}$. The experiment was repeated independently twice with similar results. **h**, Plot of ITC experiments of wild-type BAM titrated with the peptide WNWSKSF shows that there is no binding within the same concentration range as was used for darobactin. The experiment was repeated independently twice with similar results. **i, j**, Two-dimensional [^{15}N , ^1H]-TROSY spectra of 250 μM BamA- β in 0.1% w/v LDAO. **i**, BamA- β in the absence (left) and in the presence of darobactin with a molar ratio of 1:0.5 (middle) and 1:1 (right) of BamA- β :darobactin. The red dashed line outlines an example spectral region that shows substantial spectral changes during the titration. The experiment was repeated independently twice with similar results. **j**, An overlay of apo BamA- β (black) (250 μM) on BamA- β and a scrambled linear peptide WNKWSFS (green) (230 μM). The experiment was performed once.

Article



Extended Data Fig. 6 | Darobactin disrupts the outer membrane and causes lysis of *E. coli*. *E. coli* MG1655 cells were placed on top of an agarose pad that contained darobactin and the fluorescent dyes FM4-64—to stain the membrane (false-coloured in magenta)—and Sytox Green—to show membrane permeabilization (false-coloured in green). *E. coli* MG1655 cells were observed

over time at 37 °C under the microscope. For each indicated time point, representative panels show the killing progression of *E. coli* MG1655 with darobactin. White arrows highlight membrane blebbing; orange arrows highlight swelling and lysis. Scale bars, 5 μm. This figure is representative of three biologically independent experiments performed with similar results.

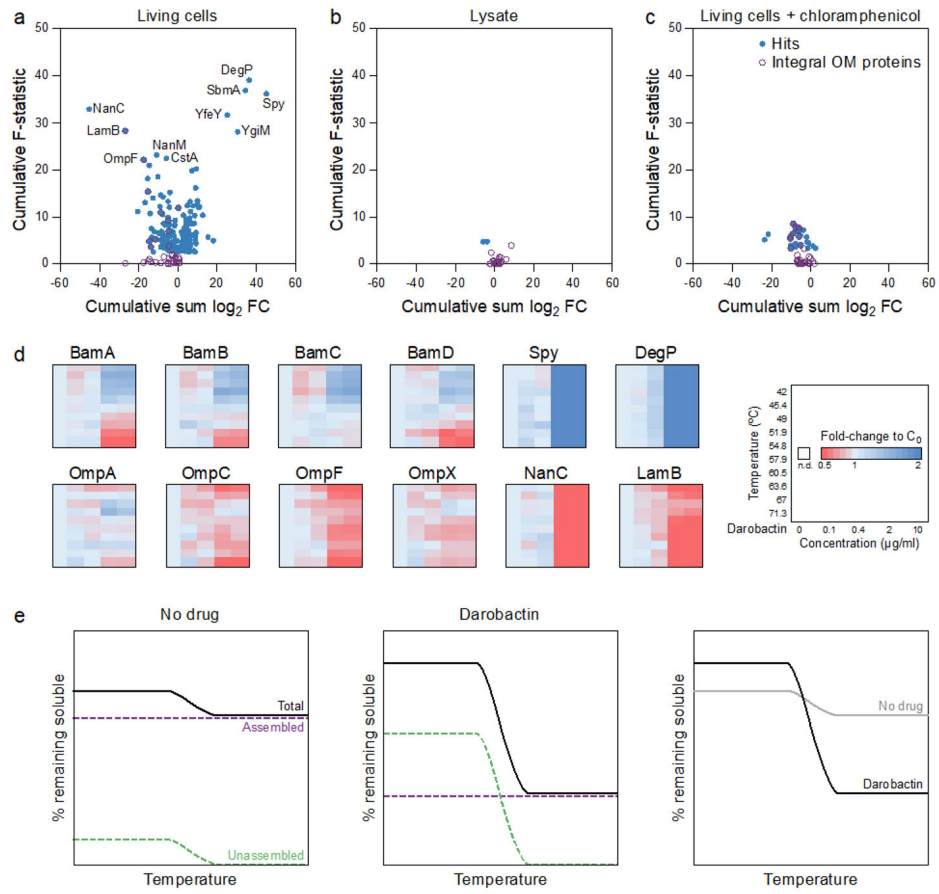


Extended Data Fig. 7 | See next page for caption.

Article

Extended Data Fig. 7 | Transcriptome analysis of darobactin treatment shows activation of envelope stress pathways. *E. coli* BW25113 were treated with 1× MIC darobactin, and the RNA isolated and sequenced. **a–c**, Volcano plots illustrate differential gene expression (Fisher's exact test in edgeR; results were deemed significant if $|\log_2(\text{FC})| \geq 2$ and FDR-corrected $P < 0.001$; $n = 3$ biologically independent samples for each control or treatment sample) at time points $t = 15$ min (**a**), $t = 30$ min (**b**) and $t = 60$ min (**c**) after exposure. Grey region, not significant. **d**, Network visualization of differentially expressed genes at each time point. Nodes include genes (coloured circles) and time

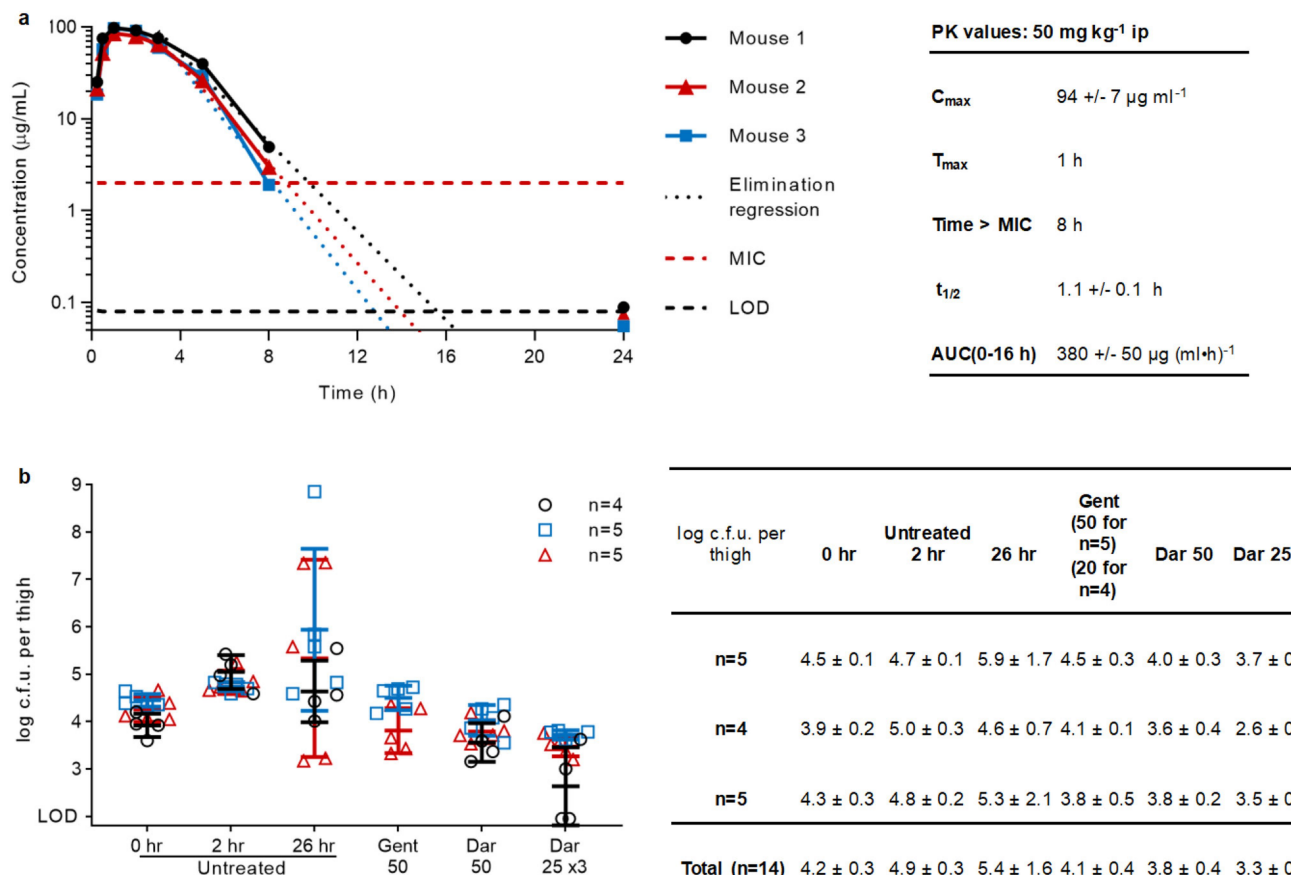
points (grey rectangles). Gene node colours represent relevant functional categories. Directed edges radiating from a time point node represent differentially expressed genes with respect to the given time point with weights reflecting the $|\log_2(\text{FC})|$. **e**, Right, heat map showing the differential expression ($|\log_2(\text{FC})|$) of genes of interest. Left, assignment to envelope stress pathways. Solid lines depict members of the same operon. In all panels, red indicates downregulation (lower expression in treatment relative to control) and blue indicates upregulation.



Extended Data Fig. 8 | Two-dimensional thermal proteome profiling of darobactin. **a–c**, Pseudo-volcano plots for two-dimensional thermal proteome profiling experiments of darobactin treatment (10 min) of *E. coli* BW25113 in living cells (**a**), lysates (**b**) and living cells pre-treated with chloramphenicol to inhibit protein synthesis (**c**). $n=1$ for each concentration, heated to 10 different temperatures, for each experiment. Significant hits (FDR-adjusted $P < 1\%$, calculated with a functional analysis of dose-response, requiring stabilization

effects at $n > 1$ temperatures as described previously⁵¹) are highlighted in blue and integral outer membrane proteins are highlighted in purple. **d**, Heat maps for selected proteins in the experiment with living cells. For each protein and temperature (a key is shown on the right), the signal intensity was normalized to the vehicle control. **e**, Schematic of putative thermally stable assembled versus labile unassembled populations of the BAM machinery with darobactin treatment.

Article



Extended Data Fig. 9 | Darobactin single-dose pharmacokinetics and mouse thigh models. **a**, Three mice were intraperitoneally injected with 50 mg kg^{-1} darobactin, and blood samples were collected by tail snip over 24 h. Samples ($n=1$ per time point and mouse) were analysed for darobactin content by LC-MS/MS, and concentrations were calculated using a standard curve created by linear regression on the log(area under the curve peak) to log(concentration) of standards. Pharmacokinetic values were calculated in Excel; $t_{1/2}$ and time > MIC assuming first-order elimination and using linear regression on

time points 3–8 h; AUC (0–16 h) using the trapezoid rule. The limit of detection (LOD) was $0.08 \mu\text{g mL}^{-1}$. **b**, A mouse thigh model was repeated three times testing the efficacy of darobactin against *E. coli* AR350. Mice were injected with bacteria in their right thigh at 0 h, then dosed with no drug, gentamicin or darobactin starting 2 h after infection (50 mg kg^{-1} once, 25 mg kg^{-1} given three times every 6 h, or 20 mg kg^{-1} once). At 26 h mice were euthanized and thighs collected and homogenized tissues were plated for c.f.u. analysis. Data are mean \pm s.d.

Extended Data Table 1 | *Photorhabdus* and *Xenorhabdus* species

<i>Photorhabdus</i> sp.	# Strains in screen	Source	<i>Xenorhabdus</i> sp.	# Strains in screen	Source
<i>P. akhurstii</i>	1	DSMZ*	<i>X. beddingii</i>	1	HGB
<i>P. caribbeanensis</i>	1	DSMZ	<i>X. bovienii</i>	12	HGB
<i>P. cinerea</i>	1	DSMZ	<i>X. douceiae</i>	1	HGB
<i>P. hainanensis</i>	1	DSMZ	<i>X. indica</i>	5	DSMZ
<i>P. heterorhabditis</i>	2	DSMZ	<i>X. innexi</i>	3	HGB and DSMZ
<i>P. kayaili</i>	1	DSMZ	<i>X. ishibashi</i>	1	DSMZ
<i>P. khanii</i>	2	HGB† and DSMZ	<i>X. japonica</i>	2	HGB and DSMZ
<i>P. kleinii</i>	1	DSMZ	<i>X. japonicus</i>	1	HGB
<i>P. laumontii</i> subsp. <i>laumontii</i>	1	DSMZ	<i>X. khoisanae</i>	4	DSMZ
<i>P. luminescens</i>	3	HGB	<i>X. miraniensis</i>	2	HGB
<i>P. noenieputensis</i>	1	DSMZ	<i>X. nematophila</i>	2	HGB
<i>P. stackebrandtii</i>	1	DSMZ	<i>X. poinarii</i>	3	HGB
<i>P. tasmaniensis</i>	1	DSMZ	<i>X. szentirmajii</i>	1	HGB
<i>P. temperata</i>	6	HGB and DSMZ			
<i>P. thracensis</i>	1	DSMZ			
<i>Photorhabdus</i> sp.	5	HGB			

*DSMZ, Deutsche Sammlung von Mikroorganismen und Zellkulturen.

†HGB, H. Goodrich-Blair.

Reporting Summary

Nature Research wishes to improve the reproducibility of the work that we publish. This form provides structure for consistency and transparency in reporting. For further information on Nature Research policies, see [Authors & Referees](#) and the [Editorial Policy Checklist](#).

Statistics

For all statistical analyses, confirm that the following items are present in the figure legend, table legend, main text, or Methods section.

n/a Confirmed

- The exact sample size (n) for each experimental group/condition, given as a discrete number and unit of measurement
- A statement on whether measurements were taken from distinct samples or whether the same sample was measured repeatedly
- The statistical test(s) used AND whether they are one- or two-sided
Only common tests should be described solely by name; describe more complex techniques in the Methods section.
- A description of all covariates tested
- A description of any assumptions or corrections, such as tests of normality and adjustment for multiple comparisons
- A full description of the statistical parameters including central tendency (e.g. means) or other basic estimates (e.g. regression coefficient) AND variation (e.g. standard deviation) or associated estimates of uncertainty (e.g. confidence intervals)
- For null hypothesis testing, the test statistic (e.g. F , t , r) with confidence intervals, effect sizes, degrees of freedom and P value noted
Give P values as exact values whenever suitable.
- For Bayesian analysis, information on the choice of priors and Markov chain Monte Carlo settings
- For hierarchical and complex designs, identification of the appropriate level for tests and full reporting of outcomes
- Estimates of effect sizes (e.g. Cohen's d , Pearson's r), indicating how they were calculated

Our web collection on [statistics for biologists](#) contains articles on many of the points above.

Software and code

Policy information about [availability of computer code](#)

Data collection

Xcalibur software (Thermo Fisher Scientific Inc.) was used for mass spectrometry analysis. Schrodinger 2018-2 was used for molecular modeling. SPAdes 3.11 was used to assemble the *Photorhabdus* genome. antiSMASH v4 was used to analyze the genome for BGCs. BLAST was used to search for homologous operons. Zen Software v14.03.201 was used to acquire fluorescent microscopy images. IsobarQuant and Mascot 2.4 were used to generate proteomic data. MassHunter B0.5 was used to quantify darobactin peaks in quantitative mass spectrometry experiments.

Data analysis

Microsoft Excel and GraphPad Prism 8.2 were used to plot graphs. Geneious 11.0.4 was used to find mutations in the resistant mutants. Fiji v1.52i software was used to process microscopy images. R v3.5.1 was used to analyze the transcriptomic and proteomic data, and Python v3.6.6 was used to plot transcriptomic data. AAT Bioquest was used to plot the BAM folding assay ITC data was analyzed and fit to the independent binding model using the NanoAnalyze software package.

For manuscripts utilizing custom algorithms or software that are central to the research but not yet described in published literature, software must be made available to editors/reviewers. We strongly encourage code deposition in a community repository (e.g. GitHub). See the Nature Research [guidelines for submitting code & software](#) for further information.

Data

Policy information about [availability of data](#)

All manuscripts must include a [data availability statement](#). This statement should provide the following information, where applicable:

- Accession codes, unique identifiers, or web links for publicly available datasets
- A list of figures that have associated raw data
- A description of any restrictions on data availability

The genome of *P. khanii* HGB1456 has been deposited to Genbank with identifier WHZZ00000000.

The transcriptomic dataset (Extended Data Figure 7) has been deposited to NCBI Sequence Read Archive with identifier PRJNA530781.

The proteomics (Extended Data Figure 8) data have been deposited to the ProteomeXchange Consortium via the PRIDE partner repository with

the dataset identifier PXD013319.

All other data available from corresponding author on reasonable request.

Field-specific reporting

Please select the one below that is the best fit for your research. If you are not sure, read the appropriate sections before making your selection.

Life sciences Behavioural & social sciences Ecological, evolutionary & environmental sciences

For a reference copy of the document with all sections, see nature.com/documents/nr-reporting-summary-flat.pdf

Life sciences study design

All studies must disclose on these points even when the disclosure is negative.

Sample size	For animal studies, sample size was chosen based on prior experience with variability between mice for infection models. For survival analysis in septicemia, three mice were used as difference in survival with treatment is dramatic. For the thigh infection model, five mice per group was used due to known variability in infection burdens in untreated mice. No sample size calculation was performed.
Data exclusions	No data was excluded
Replication	For standard microbiological assays, MICs and time-kill, experiments were done in triplicate to ensure findings were reproducible. Resistant mutants were also generated from three independent cultures. In animal studies, multiple mice were included in each group.
Randomization	Mice were randomly assigned to groups for infection and treatment, and were then housed as a group in a cage for the duration of the experiment.
Blinding	Blinding was deemed not relevant to mouse work, as outcomes were quantitative and not subjective.

Reporting for specific materials, systems and methods

We require information from authors about some types of materials, experimental systems and methods used in many studies. Here, indicate whether each material, system or method listed is relevant to your study. If you are not sure if a list item applies to your research, read the appropriate section before selecting a response.

Materials & experimental systems

n/a	Involved in the study
<input checked="" type="checkbox"/>	Antibodies
<input type="checkbox"/>	Eukaryotic cell lines
<input checked="" type="checkbox"/>	Palaeontology
<input type="checkbox"/>	Animals and other organisms
<input checked="" type="checkbox"/>	Human research participants
<input checked="" type="checkbox"/>	Clinical data

Methods

n/a	Involved in the study
<input checked="" type="checkbox"/>	ChIP-seq
<input checked="" type="checkbox"/>	Flow cytometry
<input checked="" type="checkbox"/>	MRI-based neuroimaging

Eukaryotic cell lines

Policy information about [cell lines](#)

Cell line source(s)	All cell lines were obtained from ATCC or GenTarget in 2018
Authentication	None of the cell lines were authenticated
Mycoplasma contamination	The cell lines were not tested for mycoplasma contamination
Commonly misidentified lines (See ICLAC register)	No commonly misidentified lines were used

Animals and other organisms

Policy information about [studies involving animals; ARRIVE guidelines](#) recommended for reporting animal research

Laboratory animals	Female CD-1 mice, 6 weeks old were used for all animal studies
Wild animals	The study did not involve wild animals

Field-collected samples Photorhabdus and Xenorhabdus strains were received from Heidi Goodrich-Blair, grown at 28 C on LB agar, then stored at -80 C in glycerol stocks.

Ethics oversight Animal studies were approved by the Northeastern University IACUC.

Note that full information on the approval of the study protocol must also be provided in the manuscript.